Diffusion in Charged Hydrogels

Thesis

Submitted in partial fulfillment of the
requirements for the degree of

MASTER OF SCIENCE IN PHYSICS

Author:
Johann Hansing
johannh@physik.fu-berlin.de

Supervisor:
Roland Netz
rnetz@physik.fu-berlin.de

FREIE UNIVERSITÄT BERLIN

Department of Physics

March 31, 2014

Contents

1 Introduction

Biopolymer based cross-linked hydrogels play an important role in the human body where they serve as a filter for the exchange of molecules and nanoparticles, e.g. in the form of mucus, the extracellular matrix or the biopolymer barrier in the nuclear pore complex [1–4]. Due to the importance of such biopolymer hydrogels as protective barriers against viruses, bacteria and toxic agents there has been substantial experimental research in the past few years to obtain a better understanding of the transport processes governing the diffusion of particles through biopolymer based hydrogels. Furthermore, due to good biocompatibility, synthetic hydrogels are being used as drug delivery carriers, for tissue engineering and as protein delivery systems [5, 6]. With the help of experimental techniques such as photobleaching, fluorescence correlation spectroscopy and, more recently, single particle tracking it was found that some particles (like viruses) are able to rapidly cross the hydrogel barrier, while others are immobilized [7]. In 2010, Lieleg and coworkers introduced the concept of size filtering and interaction filtering to explain the often distinct diffusivities of different particles [2]. Size filtering suggests that particles can rapidly traverse the hydrogel barrier if they are small enough to travel between the polymer chains, i.e. smaller than the average mesh size of the hydrogel. The mesh size is determined by the polymer concentration and to some extent the degree of cross-linking [8–11]. Recent experimental findings suggest however, that interactions between diffusing particle and hydrogel polymers are often even more influential on particle mobility [2, 3, 12–17]. These interactions seem to be of electrostatic nature, since the mobility is highly dependent on the particle surface charge [2, 3, 12, 14–17] and the salt concentration [2, 3]. In fact, in one study 100 nm sized, coated polystyrene beads were found to be much stronger immobilized inside undiluted human mucus than 200 and 500 nm polystyrene beads with the same coating [12]. This directly contradicts the idea that the finite mesh size of cross-linked hydrogels is solely responsible for hindered diffusion. Thus, the filtering capability of a hydrogel seems to be more dependent on nonsteric interactions between diffusing particle and hydrogel polymer, which is the concept of interaction filtering.

Our model is designed to simulate diffusion in cross-linked hydrogels of particles that are subject to interactions with the hydrogel polymers. The hydrogel structure is roughly approximated by a cubic lattice, to provide a general approximation to different types of hydrogels. The interaction potential is also a generic approximation for any kind of short-ranged interaction. This design was chosen to create a versatile

model to investigate basic mechanisms governing the diffusion of various types of particles inside cross-linked hydrogels.

1.1 Computer Simulations of Gel Networks

As outlined by Allen and Tildesley in their 1987 book "Computer Simulations of Liquids", computer simulations are a powerful tool to test physical models by comparison to analytical theories and experimental results [18]. Typically, a computer simulation may provide exact results for a problem of statistical mechanics, for which an analytical solution does not yet exist. Often, to come up with such an analytical solution for a complex problem, approximations have to be applied. A computer simulation can provide insight into which parameters are of particular importance, and which might be neglected. Also, it might provide a test to check by how much a certain approximation deviates from the exact result. If it is the aim to test how realistic a physical model is, one can compare simulation results to experiments. With a suitable model, simulations can also supplement experiments by performing virtual "computer experiments" which makes it possible to test the effect of certain experimental parameters, which might be difficult to control in a real experiment.

Various methods have been employed to simulate the diffusion of a tracer particle in charged hydrogels and complex media, such as Molecular Dynamics (MD), Monte Carlo (MC) and Brownian Dynamics (BD) simulations. Atomistically resolved MD simulations are usually based on solving the equations of motion for all N particles in the simulated system, including the water molecules, by numerical integration. This is computationally very expensive for large systems and long simulation times. Some interesting studies where MD simulations have been used to examine hydrogel properties were performed, for example, in 2009 by Wu and coworkers, who examined the effect of cross-linking on the diffusion of water, ions and molecules [19] and in 2007 by Jang and coworkers who examined the structural and mechanical gel properties as well as molecule diffusion in different hydrogels [20]. In MC simulations, the phase space is explored by randomly changing the configuration of a system. These random changes do not follow any equations of motion. In other words, an ensemble average is performed, instead of a time-average like in MD simulation. Thus, MC simulations are normally used to determine equilibrium properties of a system, e.g. the equilibrium swelling of a cross-lined polymer gel [21]. The MC method can be very useful for large systems with many degrees of freedom, since large regions of the phase space can be explored in a relatively short amount of computer time, which is

in contrast to the much slower exploration of the phase-space in MD simulations. In a Brownian dynamics simulation, the motion of the solvent particles, e.g. the numerous water molecules affecting the movement of the diffusing particle, is replaced by a combination of random forces and frictional terms in the equation of motion of the solute. This is suitable if the time scale of the dynamics of the solvent particles is much shorter than the time scale of the dynamics of interest, e.g. the long-time diffusivity of a solute. In solvent-explicit MD simulations, in contrast to solvent-implicit BD simulations, a much shorter time step would usually have to be used to correctly simulate the movement of the solvent particles, which would require a large amount of computer time. In this work, we are interested in the long-time diffusivity of a particle in a model hydrogel. Since the diffusivity is a dynamic property and since long-time behavior is of interest, a BD simulation was chosen to investigate the movement of a spherical solute particle inside our model structure.

There are a couple of studies regarding the simulation of tracer diffusion in charged and uncharged porous media and hydrogels [22–28]. Netz and Dorfmüller [22] and Miyata and coworkers [24] used linearly aligned hard-spheres which constitute a cage-like cubic lattice structure as a model environment. In a more recent paper by Zhou and Chen [25] the hydrogel structure was modeled as a network of beads which are positioned at the intersection points of a cubic lattice and connected by Hookean springs. This paper mainly focused an excluded volume effects, the network flexibility and degree of cross linking. Electrostatic interactions between particle and hydrogel has been included by Miyata and coworkers [24] as well as Zhou and Chen [25]. In both cases electrostatic interactions were found to strongly affect particle mobility but no comparisons to experimental results were drawn. Also, in the paper by Miyata and coworkers, only an oppositely charged tracer particle and hydrogel combination was investigated and the mesh size of the hydrogel was held constant. Their model predicts that attractive electrostatic interactions can slow down diffusion, especially at small ion concentrations. Stylianopoulos and coworkers [27] modeled the extracellular matrix as a spatially periodic square array of straight fibers. They included hydrodynamic interactions, as well as repulsive electrostatic interactions between a spherical tracer particle and the polymer chains and were able to predict that repulsive electrostatic interactions in combination with hydrodynamic effects can substantially slow down the mobility of nanoparticles, in qualitative agreement with experimental results for the diffusivity of nanoparticles in collagen gels. The aim of Stylianopoulos and coworkers was to create a model that is as realistic as possible while remaining computationally feasible, to be able to make concrete predictions on the optimal

design of nanoparticles for drug delivery to tumors. To achieve this, they rely on previous analytical and experimental work in the development of their model, which limits them to considering only repulsive electrostatic interactions and exploring only limited parameter ranges, e.g. for the surface potentials of the particles.

Our model consists of a spherical tracer particle diffusing in a cubic lattice comprised of straight, rigid, infinitely long rods. Nonsteric interactions between the particle and the rods are included via a general exponential potential that can be attractive or repulsive, e.g. to simulate electrostatic interactions. The goal is to focus on the key factors influencing the diffusivity of the particles inside the hydrogel, namely, short-ranged, screened electrostatic interaction, mesh size and particle size. Hence, hydrodynamic effects are neglected and a simple cubic, periodic environment is chosen to model the hydrogel polymer lattice. This serves to, on the one hand, simplify the interpretation of the results and, on the other hand, ascertain the flexibility of the model, should it need to be adjusted to probe different situations, e.g. different types of hydrogel or broader parameter ranges. Furthermore, the model is designed to be computationally inexpensive, which makes it less time-consuming to experiment with various combinations of parameters and to incorporate additional ideas. The quality of the model is tested by qualitative and quantitative comparison to experimental data. A general, qualitative comparison to experimentally determined trends, such as a decreased diffusivity for particles with larger surface charge, is followed by a closer, quantitative comparison to experimental data for a biopolymer hydrogels (mucus) as well as a synthetic hydrogel (dextran).

We find that experimentally observed trends are naturally reproduced by our model hydrogel. This includes, for example, a decreased diffusivity for particles with larger surface charge and a sensitivity for the sign of the surface charge of the diffusing particle. Furthermore, our model reproduces in trend a peculiar particle size dependency of the diffusivity of nanoparticles in mucus, where it occurs that smaller particles are more strongly hindered than larger particles. Interestingly, using different model parameters, the opposite behavior can also be reproduced, i.e. smaller particles diffusing faster than larger ones. In an analysis of the salt concentration dependency exhibited by our model simulation, we find qualitative agreement with experimental data on nanoparticle diffusion in a synthetic dextran hydrogel.

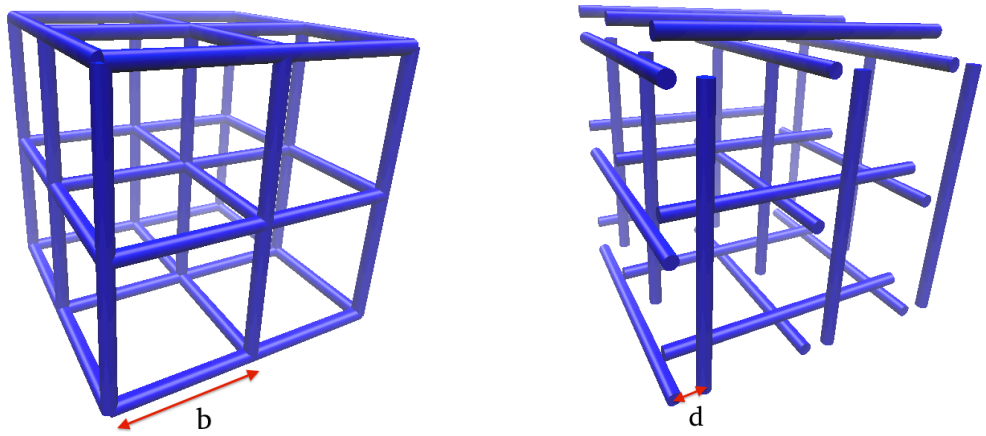

(a) Model 1

(b) Model 2

Figure 1. Schematic section of the lattice. Image **(a)** corresponds to *model 1* with nodal rod distance $d = 0$ and image **(b)** to *model 2* with $d = 0.2\,b$. The variable b is the box size. Note that the interaction range k will be given in units of b. For example, $k = 0.05\,b$ corresponds to the radius of the blue cylinders.

2 Model

In this chapter, the different models that are used to simulate a cross-linked hydrogel and a diffusing particle will be discussed. The first part focuses on modeling the hydrogel and the nonsteric interaction, the second part on the inclusion of steric effects, i.e. modeling of a finite-size particle.

2.1 Uniform Hydrogel Models

The adjective "uniform" indicates here, that the modeled hydrogel polymers are uniformly charged. This is in contrast to the random charge hydrogel model for heterogeneously charged hydrogel polymers, which will be introduced in section 2.2.

Model 1

A cubic lattice is used to model a cross-linked hydrogel comprised of polymer chains. The "rods" of the lattice represent the polymer chains and the size of a single cell b corresponds to the average mesh size of the hydrogel. Note that b stands for "box size". A sketch of the three dimensional unit cell can be found in fig. 1a. To include nonsteric interactions between a diffusing particle and the polymer chains (i.e. the

hydrogel), an exponential interaction potential is used:

$$U_I(\rho) = U_0 \exp\left(-\frac{\rho}{k}\right) , \tag{1}$$

where ρ is the distance between the particle and the rod, k is the interaction range and U_0 the strength of the potential. The subscript I stands for "interaction". For negative U_0 the potential is attractive and for positive U_0 it is repulsive. The potential only acts between particle and rod. The individual rods are static and do not interact with each other. A sketch of the interaction potential is presented in fig. 2.

A simple exponential potential has been chosen in a generic form to represent any kind of short-ranged interaction. If one thinks of electrostatic interactions, the interaction range k can be interpreted as the screening length of the potential and the strength of the potential U_0, scaled with k_BT, can be interpreted as the product of the particle charge and the polymer chain charge density. k_B is the Boltzmann constant and T the temperature. It is important to note the relative units of all variables. All spatial variables are given in units of b, i.e. relative to the box size. In the first part of this study the case of point particles will be studied. The inclusion of steric effects to study the behavior of finite-size particles is subsequently described in section 2.3.

Model 2

To avoid an unrealistically strong interaction potential at the intersections of the rods, the rods are displaced by a distance d at the nodal crossing points, such that the potential minima of the individual rods do not overlap anymore in the corners of the simulation box. A sketch of how such a lattice looks for $d = 0.2\,b$ can be found in fig. 1b. Note that the box size b (i.e. the mesh size) is the same as in model 1.

Model 3

Another approach to avoid a very deep potential minimum at the intersections is to modify the potential with a weighting function, such that the potential of a single rod decreases towards the intersections of the rods:

$$U_{\mathrm{mod}}(\rho, z) = U_I(\rho) \cdot \left[1 - \left|\frac{2z}{b} - 1\right| \frac{2}{3}\right] . \tag{2}$$

Here, ρ and z are cylindrical coordinates and the axis of the rod is along z. Thus, the potential is reduced to $1/3$ of U_0 at $z = 0,\ 1\,b$, i.e. at the corners of the simulation

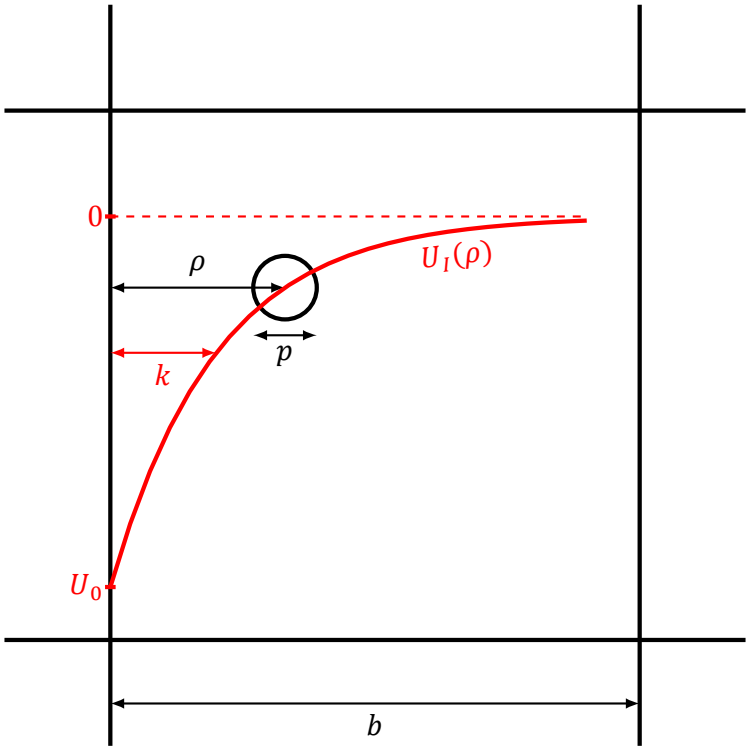

Figure 2. Schematic section of the lattice in a 2D projection with indicated attractive interaction potential of the left rod. The shape of the full interaction potential with contributions from all rods is presented in figs. 12a and 12b.

box. A plot of the weighing function is shown in fig. 3.

2.2 Random Charge Model

Experimental research by Lieleg and coworkers on diffusion in mucus hydrogels has shown that particles with a stronger surface charge are usually more strongly immobilized in mucus than particles with a weaker surface charge [2, 3]. This holds for positively and negatively charged particles alike which is why it is suggested in the same studies, that the mucus polymer chains consist of sections of alternating charge, as indicated in fig. 4a. To account for such an effect in our simulations we devised the *random charge model* explained in the following: The hydrogel model 1 described above is altered to include varying patches of attractive and repulsive interaction with the particle. This is realized in a manner as simple as possible, namely, by randomly assigning a charge of $\sigma_i U_0$ to each edge i of the simulation box, where σ_i is randomly set to either 1 or -1, with equal probability. Thus, σ_i can be interpreted as the sign

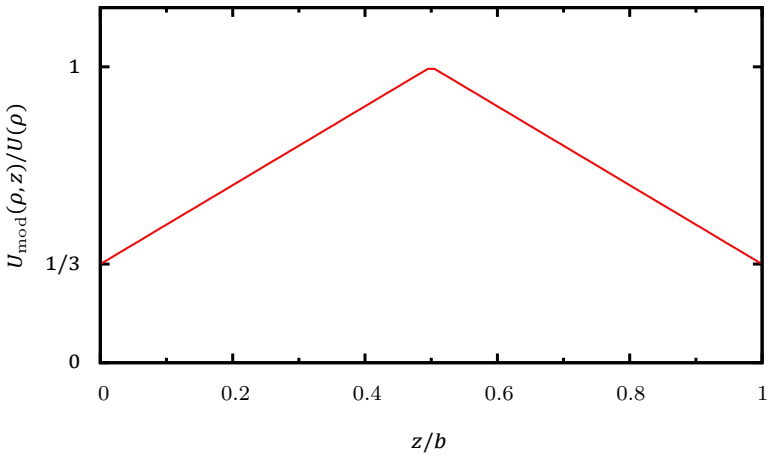

Figure 3. Potential modification function as used in eq. (2).

of the surface charge of the ith simulation box edge. A sketch of a two dimensional projection of the random charge model polymer lattice can be found in fig. 4b.

To avoid strong discontinuities in the force field inside the polymer lattice, the potential strength U_0 goes to zero at the transition between two oppositely charged patches along the polymer chain. This is done by linear interpolation between a state $+\sigma$ and a state $-\sigma$ in a range of $\frac{1}{4}b$, as shown in eq. (3), i.e. by multiplying the interaction potential $U_I(\rho)$ with a z-dependent factor, where z and ρ are cylindrical coordinates and the z-axis is aligned along the polymer chain axis, as indicated in fig. 4c.

$$U_i^{\mathrm{ran}}(\rho,z) = \sigma_i U_I(\rho) \times \begin{cases} \frac{4z}{b}, & 0 < z < b/4 \text{ and } \sigma_i \neq \sigma_{i-1}\,, \\ \frac{4(b-z)}{b}, & 3b/4 < z < b \text{ and } \sigma_i \neq \sigma_{i+1}\,, \\ 1\,, & \text{else}\,. \end{cases} \tag{3}$$

Here, $U_i^{\mathrm{ran}}(\rho,z)$ is the potential of a single polymer chain interval i, σ_i corresponds to the sign of the interaction potential of polymer chain interval i and σ_{i-1} and σ_{i+1} to that of the neighboring polymer chain intervals along the same polymer chain as indicated in figs. 4b and 4c. This linear interpolation is of course only a rough approximation that serves to keep the model simple.

During the simulation, only the rod intervals that lie within the box indicated in fig. 4b have an actually determined potential sign σ. All rod intervals outside the simulation box only get a σ assigned, if the particle diffuses into a neighboring box. Also; the system "forgets" the sign σ of previously assigned rod patches, as soon as they

do not lie within the simulation box anymore. In other words: Only the rod intervals necessary to compute eq. (3) are determined during the simulation, e.g. $i + 1$ and $i - 1$ indicated in fig. 4b. A "memory" for previously assigned rod intervals should not substantially change the results of the simulation due to the random nature of the assignment of the σ values.

2.3 Steric Effects

Here, we investigate how the long-term relative diffusivity D/D_0 is affected by including steric effects, i.e. by switching from point particles to spheres of a finite-size p. The variable p stands for "particle size" as it corresponds to the diameter of the particle. This is mainly motivated by the experimental findings that 100 nm coated polystyrene beads were found to be much stronger immobilized than 200 and 500 nm polystyrene beads with the same coating inside undiluted human mucus [12], which indicates, that in some cases diffusion effects in hydrogels can only be explained by a combination of electrostatic and finite-size effects.

Hardcore Potential 1

A hardcore potential is included in such a way that whenever the particle moves a step it is first tested whether the minimum distance between the particle and any of the 12 rods is smaller than the particle radius. If so, the particle is returned to its previous position, the random force regenerated and the procedure repeated. Only if the check comes back negative, i.e. if the particle does not overlap with any rod, the particle configuration is adopted and a time step added. This method might lead to an overestimation of the diffusion because if the particle is being moved somewhere it can not be, i.e. if it encounters an obstacle, it does not stop, but rather instantaneously changes its direction of movement. In other words, the particle always just flows around the polymer and never hits it. To estimate this effect, another very similar hardcore potential is also tested for comparison, which is described in the next section.

Hardcore Potential 2

In another version of the aforementioned hard sphere interaction a time step is added, even if the particle is not moved, due to overlap. This serves to simulate the possibility of the particle getting stopped by steric interactions. This method is similar to

(a) Lieleg and coworkers model structure.

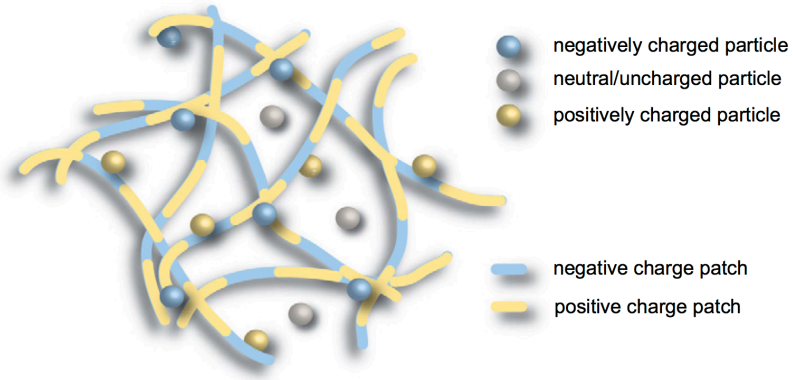

(b) Random charge model structure.

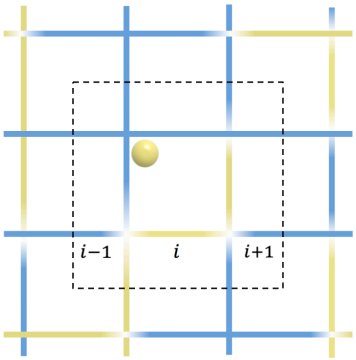

(c) Potential along the rod i.

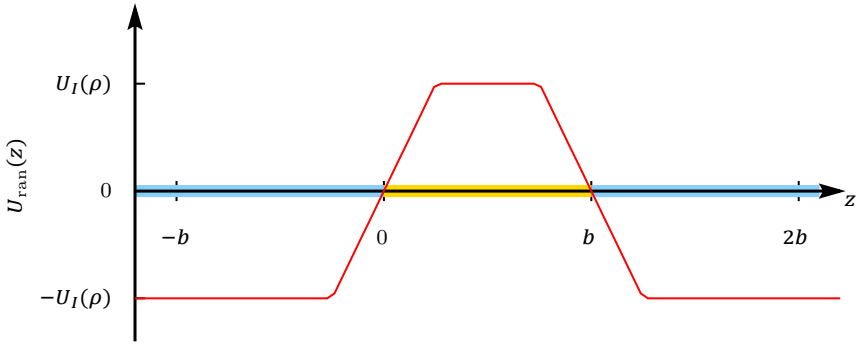

Figure 4. Figure **(a)** shows a sketch created by Lieleg and coworkers [3]. It indicates their suggestion for the charge distribution inside an extracellular matrix hydrogel. Charged particles are immobilized because they *stick* to oppositely charged patches of the hydrogel polymer chains. This is the experimental basis of the random charge model introduced in section 2.2. A 2-dimensional projection of the random charge model structure is shown in **(b)**. Here, the simulation box is indicated by the dashed square. Charged particles should experience an attraction to oppositely charged polymer chain intervals. This is indicated by the yellow circle (the particle) being near the blue polymer chain intersection, with the colors corresponding to opposite charges. The potential $U_i^{\mathrm{ran}}(\rho, z)$ (c.f. eq. (3)) along the lowermost rod is sketched in **(c)**. The z-axis lies along the polymer chain. For a positively charged particle, the blue color indicates a repulsive polymer chain region, the yellow color an attractive. The red line indicates the shape of the potential at constant distance ρ between polymer chain and diffusing particle.

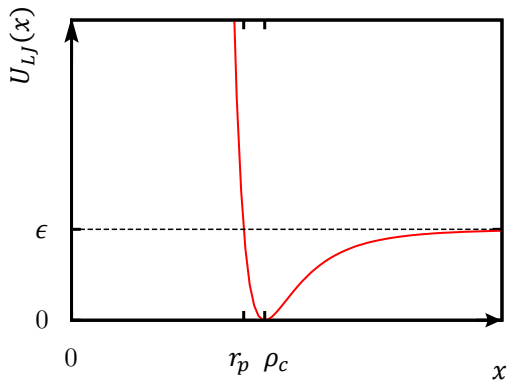

Figure 5. Sketch of the shifted Lennard-Jones potential introduced in eq. (4). Note that this sketch shows the full Lennard-Jones potential. The potential used in the simulations is truncated at $x = \rho_c$.

the method used in the simulations by Miyata and Netz [22, 24]. The two different simulation methods are compared in the Results (section 4).

Truncated Lennard-Jones Potential

Another approach to include steric effects is to include a shifted and truncated Lennard-Jones (LJ) potential similar to the one employed by Zhou and Chen [25]:

$$U_{\mathrm{LJ}}(\rho) = \begin{cases} 4\epsilon \left[\left(\frac{p}{2\rho}\right)^{12} - \left(\frac{p}{2\rho}\right)^{6} + \frac{1}{4} \right], & \rho \leq \rho_c \,, \\ 0 \,, & \rho > \rho_c \,, \end{cases} \tag{4}$$

where the energy depth is $\epsilon = 1\ k_B T$, $r_p = \frac{p}{2}$ the particle radius and ρ the distance between the particle center and the rod. The potential is truncated at the cutoff distance $\rho_c = \sqrt[6]{2}\, r_p$, which corresponds to the value of ρ at which the LJ potential has its minimum, as shown in fig. 5.

2.4 The Debye-Hückel Potential

Electrostatic interactions between charged particles in electrolyte solutions can be described approximately by the Debye-Hückel potential [29]

$$U_{\mathrm{DH}}(r) = \frac{Q_i Q_j}{4\pi\epsilon} \frac{\exp(-r/k)}{r} \,. \tag{5}$$

Here, Q_i and Q_j are the charges of the involved particles, ϵ the solvent dielectric constant and the screening length k is given by

$$k^2 = \frac{\epsilon\epsilon_0\, k_B T}{2e^2 I} \,, \tag{6}$$

where e is the elementary charge and $I = \frac{1}{2}\sum_j n_j z_j^2$ the ionic strength, z the valence of the salt ions and n_i their bulk number densities. Rearranging this formula and switching from number densities n to molar concentrations C leads to the following expression for a monovalent electrolyte solution in water ($\epsilon = 80$) at room temperature $T = 25^\circ C$ [29]:

$$k = \frac{0.304\,\mathrm{nm}}{\sqrt{I/\mathrm{M}}}\,, \tag{7}$$

$$C_\mathrm{s} = \frac{0.092\,\mathrm{nm}^2\,\mathrm{M}}{k^2}\,, \tag{8}$$

where C_s is the salt concentration in molar and k the interaction range of the exponential potential (c.f. eq. (1)) in units of nm. This connection between salt concentration C_s and interaction range k is used to calculate the salt dependency of the simulation data.

2.5 Maxwell-Boltzmann Statistics

Noninteracting, classical particles in thermal equilibrium follow Maxwell-Boltzmann (MB) statistics. From this, one can calculate the probability of finding a particle in a certain energy state. Consider a dilute concentration of particles in a solution, which experience different potential energies u_1 and u_2 in two different regions inside the solution, e.g. in our hydrogel model, near a rod intersection or the center of the simulation box. The respective concentrations C_1 and C_2 in those regions, are given by the MB distribution [29]:

$$C_1 \mathrm{e}^{-u_1/k_BT} = C_2 \mathrm{e}^{-u_2/k_BT}\,. \tag{9}$$

These differences in concentration can be readily translated into a probability density $p(\vec{r})$ of finding the particle at a certain position $\vec{r}$ in the simulation box:

$$p(\vec{r}) = \frac{\mathrm{e}^{-U(\vec{r})/k_BT}}{\int_{V_\mathrm{box}} \mathrm{d}^3 r\, \mathrm{e}^{-U(\vec{r})/k_BT}}\,, \tag{10}$$

where V_box is the volume of the simulation box, which the expression in the denominator is integrated over and $U(\vec{r})$ the total potential of the particle at position $\vec{r}$. Equation (10) can be used to numerically calculate some average properties of the

model, like the mean potential energy of particle inside the simulation box:

$$\langle E_{\mathrm{pot}} \rangle = \int_{V_{\mathrm{box}}} \mathrm{d}^3 r \; p(\vec{r}) \; U(\vec{r}) \; . \tag{11}$$

The numerical integration is performed with the MATHEMATICA software using the built in function `NIntegrate`. The results of this numerical integration can be compared to the simulation output as a validity check, since the results of the BD simulation should be in agreement with the MB statistics.

3 Brownian Dynamics Simulation

The motion of a particle inside a fluid is governed by random collisions with the molecules or atoms of the fluid. These random "bumps" create a diffusive motion of the particle, which is called *Brownian motion*. The name stems from Scottish botanist Robert Brown who published a study about the jittery motion of pollen suspended in water in 1827.

3.1 The Langevin Equation

Brownian motion can be modeled in terms of a stochastic differential equation, the so-called *Langevin* equation:

$$m\,\ddot{r}_i(t) = -\lambda\,\dot{r}_i(t) + \mathrm{Z}_i(t)\,, \quad (i = x, y, z)\,. \tag{12}$$

The Langevin equation is an equation of motion where the rapid, random collisions are included via an instantaneous random force $\vec{\mathrm{Z}}(t)$ acting on the particle at position $\vec{r}$ with mass m and a friction coefficient λ. The dot indicates a time derivative. If the particle is also subject to a force field one can simply add the forces $\vec{f}(t) = \vec{\nabla}U(\vec{r}(t))$ acting on the particle to eq. (12). Furthermore, one can neglect the acceleration term $\ddot{r}(t)$, if the long-time configurational dynamics are of interest [18], which leads to the so-called *overdamped Langevin equation*. This approach is valid as both the overdamped and the classical Langevin equation (eq. (12)) fulfill Einstein's relation (c.f. eq. (21), which describes the long-time diffusivity. Accordingly, the resulting (overdamped) Langevin equation is the basis for our simulations:

$$\dot{r}_i(t) = -\mu_0\,\nabla_i U(\vec{r}(t)) + \zeta_i(t)\,, \quad (i = x, y, z)\,, \tag{13}$$

where $\dot{r}_i$, ∇_i and ζ_i are the time derivative of the particle position, the spatial derivative, and a random velocity in i-direction, respectively. U is a potential, t the time and μ_0 the bulk sphere mobility $\mu_0 = 1/(3\pi\eta p)$ derived from Stokes' law, where η is the dynamic viscosity of the solvent and p the particle diameter. The random velocity ζ_i is a stochastic variable, modeled with Gaussian white noise

$$fir\langle\zeta_i(t)\rangle = 0\,, \tag{14}$$

$$\langle\zeta_i(t)\,\zeta_j(t')\rangle = 2\mu_0 k_B T\,\delta(t - t')\,\delta_{ij}\,. \tag{15}$$

By integrating both sides of the Langevin equation (eq. (13)) from t to $t + \Delta t$, one arrives at a discrete, iterable expression for the particle position:

$$\begin{aligned}
\tilde{r}_i(t+\Delta t) - \tilde{r}_i(t) &= \int_t^{t+\Delta t} \left(-\frac{\mu_0\, k_B T}{b^2}\, \tilde{\nabla}_i \tilde{U}(\tilde{r}_i(t')) + \frac{\zeta_i(t')}{b} \right) \mathrm{d}t' \,, \\
\tilde{r}_i(t+\Delta t) - \tilde{r}_i(t) &\approx -\Delta t\, \frac{\mu_0\, k_B T}{b^2}\, \tilde{\nabla}_i \tilde{U}(\tilde{r}_i(t)) + \int_t^{t+\Delta t} \frac{\zeta_i(t')}{b}\, \mathrm{d}t' \,, \\
\tilde{r}_i(t+\Delta t) - \tilde{r}_i(t) &= -\tilde{\mu}\, \tilde{\nabla}_i \tilde{U}(\tilde{r}_i(t)) + \sqrt{2\tilde{\mu}}\, \tilde{\zeta}_i(t) \,. \qquad (16)
\end{aligned}$$

The tilde stands for a rescaled variable. All lengths are scaled by the box size b and energies by the thermal energy $k_B T$. The rescaled random velocity $\tilde{\zeta}$ is a Gaussian distributed random number with 0 mean and variance 1. The pseudo random number generator used for the simulations is the Mersenne twister generator [30] included via the boost C++library package.

The rescaled timestep $\tilde{\mu}$ is defined as

$$\tilde{\mu} = \frac{\Delta t\, \mu_0\, k_B T}{b^2}. \qquad (17)$$

In accordance to the flow chart in fig. 6 depicting the fundamental procedure of a BD simulation step, expression 16 will be used to update the particle position $\vec{r}(t)$ recursively. To avoid the particle taking too large steps which would distort the results of the simulation, the rescaled timestep $\tilde{\mu}$ should be chosen small enough so the displacement of the particle in every iteration step calculated from eq. (16), is small compared to the particle radius, or, for point particles, small enough such that the simulation data does not change upon choosing a smaller timestep. In the test simulations, this could be achieved with a rescaled timestep of $\tilde{\mu} = 0.0005$. For the simulations in this work a timestep of $\tilde{\mu} = 0.0001$ is used, which is even lower, to assure results that correspond to the long-time limit.

3.2 The Total Interaction Potential

In eq. (16) the total potential $U(\vec{r})$ that acts on the diffusing particle is

$$U(\vec{r}) = U^{\mathrm{i}}(\vec{r}) + U^{\mathrm{s}}(\vec{r}) \,. \qquad (18)$$

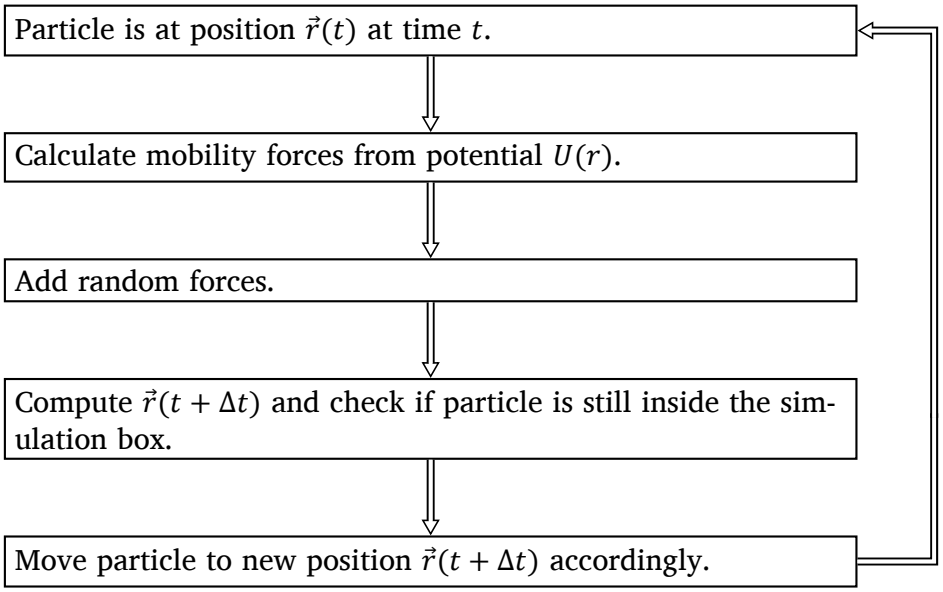

Figure 6. Flowchart for one simulation step of the BD simulation.

where the subscripts s and i denote the total steric and nonsteric interactions, respectively, i.e.

$$U^{\mathrm{i}}(\vec{r}) = \sum_{n=1}^{N} U_I(\rho_n)\,, \tag{19}$$

in the hydrogel model 1 case. The index n denotes the contributions to the total potential by the individual rods and ρ_n is the radial distance between the particle and the nth rod. For computational efficiency the summation is limited to a finite number of N nearest neighbor rods. A *first order* summation includes $N = 12$ rods, i.e. those rods at the edges of the simulation box. A *second order* summation includes $N = 48$ rods, which also includes the contributions of the rods at the edges of the adjacent unit cells. For the investigated interaction ranges k going from $k = 0.01\,b$ to $k = 0.5\,b$ it is sufficient to include the rods to first order for ranges $k < 0.2\,b$ and to second order for ranges $k \geq 0.2\,b$, since the contributions of higher order rods are negligible for these ranges k. Only the random charge model described in section 2.2 poses a special case. Here, the potential is only summed to first order and therefore the interaction ranges k only investigated up to $k = 0.35\,b$, since the discussion is focused on behavior on shorter interaction ranges, and for the sake of efficiency.

In eq. (18) hydrodynamic effects are disregarded. Hydrodynamic effects are of

long-range nature, so they would pose a computationally expensive addition to the model, whose simplicity and computational efficiency is a key factor. Furthermore, the model is designed as a strong simplification of the realistic scenario of particle diffusion in hydrogels, with a focus on electrostatic interactions between hydrogel and particle.

3.3 The Diffusion Parameter

The diffusion parameter D is the response coefficient of the diffusing particle, defined by [18]

$$D = \frac{1}{3}\int_0^\infty \mathrm{d}t\langle\vec{v}(t)\cdot\vec{v}(0)\rangle \tag{20}$$

where, $\vec{v}(t)$ is the velocity of the diffusing particle. For large t the Einstein relation holds, which, in three dimension, leads to the expression

$$2tD = \frac{1}{3}\langle|\vec{r}(t)-\vec{r}(0)|^2\rangle\,, \tag{21}$$

Therefore, in the long-time limit the mean square displacement (MSD) of the particle becomes proportional to the diffusion parameter D

$$\lim_{t\to\infty}\langle\Delta r^2(t)\rangle = 6\,D\,t\,. \tag{22}$$

The diffusivity D of the particle is obtained by linearly fitting the MSD in the long-time limit. To obtain a good mean, the average is calculated over 10000 simulation runs. To test whether the linear fit is indeed taken in the long-time limit, the coefficient of determination R^2 of the fit is extracted from the linear fit output. The coefficient of determination is defined as $\mathrm{R}^2 = 1 - SS_{\mathrm{res}}/SS_{\mathrm{tot}}$, where SS_{res} is the sum of squares of residuals with respect to the linear regression and SS_{tot} the total sum of squares. A value of $\mathrm{R}^2 = 1$ indicates that all points used for the regression lie on the regression line. Hence, if the we start linearly fitting our MSD data before the long-time limit R^2 will be considerably smaller than 1, since before the long-time limit, the MSD does not increase linearly in time. The initial fit of the data starts at a time $t = 100$. We then use an automated script to check that R^2 of that fit is larger than 0.9. If that is not the case, the fit is repeated, starting at from a larger t value. This process is repeated until the condition $\mathrm{R}^2 > 0.9$ is met.

The diffusion parameter for a freely diffusing particle without any kind of interac-

tions is D_0, i.e. the free diffusion coefficient for diffusion in water. It is determined by the Stokes-Einstein equation, $D_0 = \mu_0 \, k_B T$. Most of the results are presented in terms of the relative diffusivity D/D_0 to show how much the particle diffusion is inhibited inside the hydrogel. The error of the relative diffusivities is estimated to be $\Delta(D/D_0) = \pm(5\% + 0.0002)$. It consists of a relative and an constant part since we observed that larger D/D_0 values fluctuate more strongly than smaller ones for different runs with identical parameters. This issue is more closely discussed in the results section 4.1 where some concrete examples of what the simulation data look like are shown and explained. The magnitude of the error is determined by comparing limiting cases of the simulation and the respective fluctuations of D/D_0, i.e. cases of very strong hindrance due to interactions and cases of almost free diffusion.

The Standard Deviation

The standard deviation X can be used as a measure of the dispersion of a statistical quantity Q around its mean $\bar{Q}$. It is defined as

$$X = \sqrt{X^2} = \sqrt{\frac{1}{n-1} \sum_{i=1}^{n} \left(Q_i - \bar{Q}\right)^2}, \tag{23}$$

where n is the number of sampling points. In this work, the standard deviation is employed to compute the error of the MSD in the simulation output. In this context it is also referred to as *standard error*.

4 Results

In this section, we present the results of the systems introduced above. First, the direct output of the simulations is discussed. Subsequently, we will turn to the diffusivity of point particles in the three hydrogel models that are introduced in section 2.1 and of finite-size particles in a hydrogel of the model 1 type.

4.1 Simulation Output

Some exemplary output of the simulation is shown in figs. 7 and 8. All simulation data is recorded at a timestep of $\tilde{\mu}_0 = 0.0001$ and mean values are averaged over at least 10000 particle runs. To avoid correlations due to resetting the particle to its original starting position in the center of the simulation box, we perform continuous runs which are split into several thousand sub-trajectories. Figure 7a shows exemplary MSD output, which is found to increase linearly in time, as expected. The errors of the MSD data points correspond to their standard deviation, introduced in eq. (23). In fig. 7b, which shows the same MSD data divided by time as a function of the simulation time, one can see that the these ratios approach a constant value in the long-time limit. This is the expected behavior, as explained in section 3.3. At short time scales the hindered diffusion of the Brownian particle is anomalous [23], i.e. the MSD does not increase linearly in time. One can see this non-linear behavior in fig. 7b where, for example, the data for $U_0 = -5\,k_BT$ initially decreases. To reach long-time diffusivity, the MSD of a particle usually needs to be larger than at least the box size squared, i.e. $\mathrm{MSD}/b^2 > 1$. This can be observed by comparing fig. 7a to fig. 7b. For example, the $U_0 = -5\,k_BT$ data exhibits long-time diffusivity for $t > 30$, which corresponds to the time by which MSD/b^2 becomes greater than 1 in fig. 7a. According to eq. (22), one has to divide the long-time slope by a factor of 6 to obtain the relative diffusivity D/D_0 of the diffusing particle. For the given examples, the resulting values fo D/D_0 are shown in table 1.

As shown in fig. 7b the $U_0 = -5\,k_BT$ data has smaller errors and fluctuates less strongly than, e.g. the $U = -1\,k_BT$ data. This is because at $U_0 = -5\,k_BT$ the particle experiences a stronger force field, which counteracts the random directionality of the Brownian motion. A particle experiencing a weak potential can fluctuate freely, whereas a particle experiencing a strong potential is more restricted in its mobility. Since, the error of the MSD data is the standard deviation, stronger fluctuations lead to larger error intervals, which is why the error intervals for the data in fig. 7 are largest for the smallest potential strength $U_0 = -1\,k_BT$. An interesting aspect of our

Table 1. The long-time slopes and respective relative diffusivities of the data shown in figs. 7 and 8. The errors of the slopes are the error estimates returned by the gnuplot software, which uses an implementation of the nonlinear least-squares Marquardt-Levenberg algorithm for fitting [31]. The errors are the standard errors of the fit parameters and are, in general, not to be understood as confidence intervals. Thus, the errors of the relative diffusivities correspond to the gauged error introduced in section 3.3, which is a considerably larger relative error than the relative error of the slopes.

potential strength $U_0/\,k_BT$	-1	-5	5
slope	5.89 ± 0.01	0.2354 ± 0.0006	5.151 ± 0.006
relative diffusivity D/D_0	0.982 ± 0.05	0.03923 ± 0.002	0.8585 ± 0.05

model can already be observed here, namely, that attractive and repulsive potentials of equal absolute potential strength $U_0 = -5$ and $+5\,k_BT$ lead to different diffusivities. This will be more closely examined in section 4.2.

Figure 8 shows the mean potential energy $\langle E_{\text{pot}}\rangle/\,k_BT$ during the same set of simulations which are presented in fig. 7. The mean potential energy remains constant throughout the simulation which indicates accuracy of the simulation results. A closer examination of the mean potential energy of the diffusing particle for different ranges k and potential strengths U_0 can be found in section 4.2.

4.2 Point Particles

For the simulated diffusion of infinitely small particles, i.e. point particles, the only relevant tunable parameters are the potential strength $U_0/\,k_BT$ relative to the thermal energy and the interaction range k/b relative to the box size. In fig. 9a, the dependency of the relative diffusion coefficients D/D_0 on the potential strength U_0 is presented for different k, indicated by differently colored curves. The curves are shown for a range $-10\,k_BT \leq U_0 \leq 20\,k_BT$. Here, they show small relative diffusivities near zero at $U_0 = -10\,k_BT$ up to a value of $D/D_0 = 1$ at $U_0 = 0$, which implies free diffusion, as expected for point particles at zero potential strength. From there, the relative diffusivity decreases again for increasing U_0 with a different degree of shrinkage for different interaction ranges k. In the attractive regime (negative U_0) the relative diffusivity changes considerably even for small variations of $\pm 1\ k_BT$ in potential strength. This is due to a strong potential minimum near the intersections of the rods, where the contributions to the potential of three rods add up. If the particle diffuses into such a quite localized minimum it will have a tendency to "stick" there. This effect will henceforth be referred to as *sticking*. In the repulsive regime a

(a) MSD data example

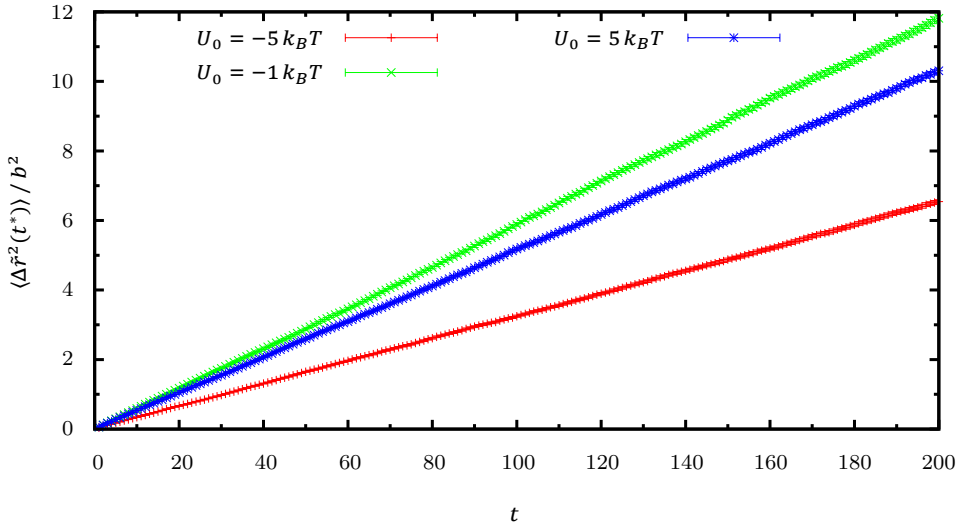

(b) MSD/t data example

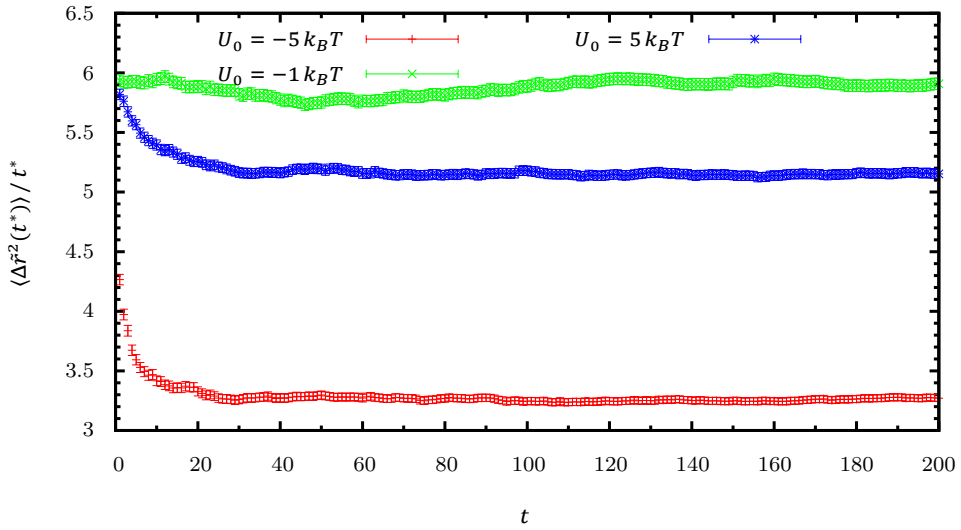

Figure 7. Typical MSD simulation data output for different potential strengths U_0. All the data above has been recorded for point particles in hydrogel model 1 (c.f. section 2.1) and at constant interaction range $k = 0.1\,b$ with a timestep of $\tilde{\mu}_0 = 0.0001$ and averaged over 10000 simulation runs. Plot **(a)** shows the MSD, $\langle \Delta\tilde{r}^2(t)\rangle$, plotted in dependence of the simulation time t. Plot **(b)** shows the same data but with the MSD divided by the simulation time, to show how it approaches a constant value in the long-time limit, as introduced in section 3.3. This long-time value, divided by a factor of 6, corresponds to the relative diffusivity D/D_0 of the particle, where the division by 6 follows from eq. (22).

trapping effect occurs, where the particles tend to be "pushed" by the repulsive interactions into the potential minimum in the center of the box, but only at much larger absolute potential strengths. This effect also manifests in the shape of the mean potential energy $\langle E_{\text{pot}} \rangle$ as a function of potential strength U_0 shown in fig. 9b. For all presented interaction ranges k the mean potential energies decrease strongly towards negative U_0. For short interaction ranges $k = 0.05\,b$ to $0.2\,b$, the mean potential energies approach a value of almost $\langle E_{\text{pot}} \rangle = -30\,k_B T$ which corresponds to three times the potential strength $U_0 = -10\,k_B T$ of an individual rod. This indicates, that the particle tends to stick to the intersections in the corners of the simulation box, where it experiences the full potential strength of three rods. For larger interaction ranges the $\langle E_{\text{pot}} \rangle$ value at $U_0 = -10\,k_B T$ is larger due to contributions of neighboring rods, which are considerable for interaction ranges larger than $k > 0.2\,b$. For increasing positive U_0, the $k = 0.05\,b$ and $0.1\,b$ data remain almost constant near zero due to the particle spending most time near the center of the box, far away from the potential maxima. In contrast to the data for small ranges k, the curve for $k = 0.5\,b$ has almost the same shape in the attractive and in the repulsive regime. Thus, the dissimilarity between the shape of the curves in the different regimes indicates how strongly the diffusive behavior differs in the attractive and repulsive cases. This effect can be also

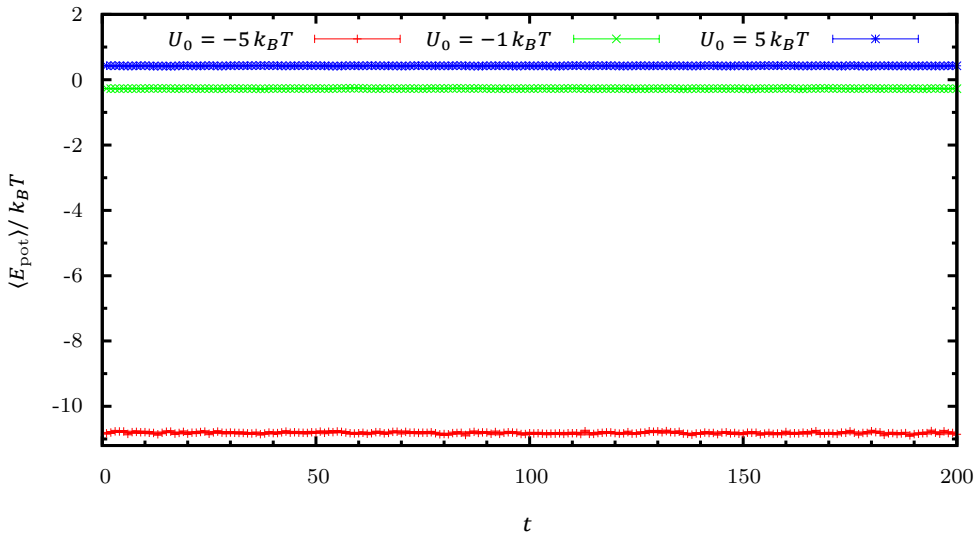

Figure 8. Mean potential Energy $\langle E_{\text{pot}} \rangle$ of a particle during exemplary simulations at different potential strengths U_0 in dependence of the computer time t. The data shown is obtained from the same simulation runs as the MSD data shown in fig. 7, i.e. for point particles in hydrogel model 1 (c.f. section 2.1) and at constant interaction range $k = 0.1\,b$ with a timestep of $\tilde{\mu}_0 = 0.0001$. One can see, that the potential energy remains constant on average during the simulation.

be observed by examining the $k = 0.05\,b$ curve in fig. 9a. Here, the relative diffusivity starts to decrease rapidly at $U_0 = -3\,k_BT$ towards stronger negative U_0. This rapid decrease manifests in fig. 9b in the form of a "dent" in the $k = 0.05\,b$ curve at $U_0 = -3\,k_BT$. Trapping and sticking can also be observed in the contour plots in fig. 10, where the colors indicate the probability of finding the particle. Even for a relatively weak attractive potential with $U_0 = -3\,k_BT$, the particle has a very small, even negligible probability to be in the center of the box, compared to being localized in one of the eight corners. Near an attractive rod connecting two corners, the probability is very low (only light coloring). This indicates, that the particle traverses the network by "jumping" between intersections.

For an equally repulsive potential $U_0 = 3\,k_BT$, the probability distribution inside the box is much more homogeneous. The particle spends more time in the center of the box, far away from the rods. This shows that the particle is indeed sticking to the corners for negative U_0 or, although much less strongly, trapped in the center of the box for positive U_0. From the plane 2 plots in fig. 10 one can see that the particle mostly travels between boxes through the centers of the sides if the interaction potential is repulsive.

Another trait of the model which can be observed in fig. 9a is that, in the repulsive regime ($U_0 > 0$), the diffusivity is most sensitive to increasing U_0, when the interaction range is $k = 0.3\,b$. This effect can be observed even more clearly in fig. 11, which shows the relative diffusivity D/D_0 in dependence of the interaction range k. Here, a clear minimum can be seen at $k = 0.3\,b$ in the repulsive regime (for positive U_0). For increasing ranges larger than $k = 0.3\,b$ the potential difference between the center of the box and the sides of the box starts to decrease again. In the contour plot in fig. 10f we see that the potential barrier between box side and center, is the barrier the particle usually crosses to move between adjacent boxes. Thus, an increasing potential barrier leads to a decreasing diffusivity and a decreasing potential barrier to a increasing diffusivity. The shape and height of the potential barrier between simulation box center and side is shown in fig. 12a and fig. 12c, respectively. One can see a clear maximum in fig. 12c at $k = 0.3\,b$, which corresponds to the aforementioned minimum in relative diffusivity for repulsive potentials in fig. 11, which also lies at $k = 0.3\,b$.

A minimum is also visible in the attractive case of $U_0 = -5\,k_BT$ in fig. 11 at an interaction range of $k = 0.15\,b$. The D/D_0 values for $U_0 = -10\,k_BT$ at small k are very close to zero, thus if there is a minimum, it is below the resolution of the simulation, or at an interaction range lower than $k = 0.1\,b$, which would require a smaller time

(a) Relative diffusivities

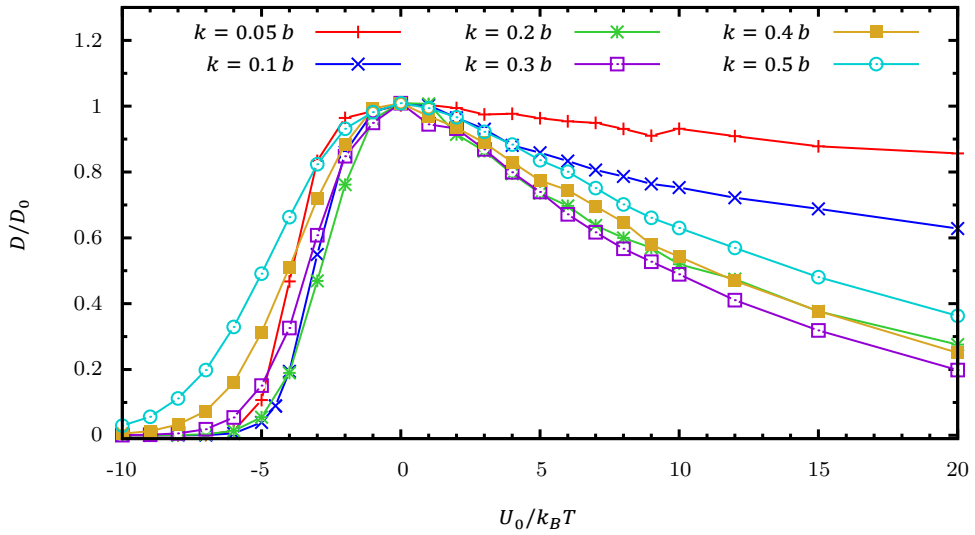

(b) Mean potential energies

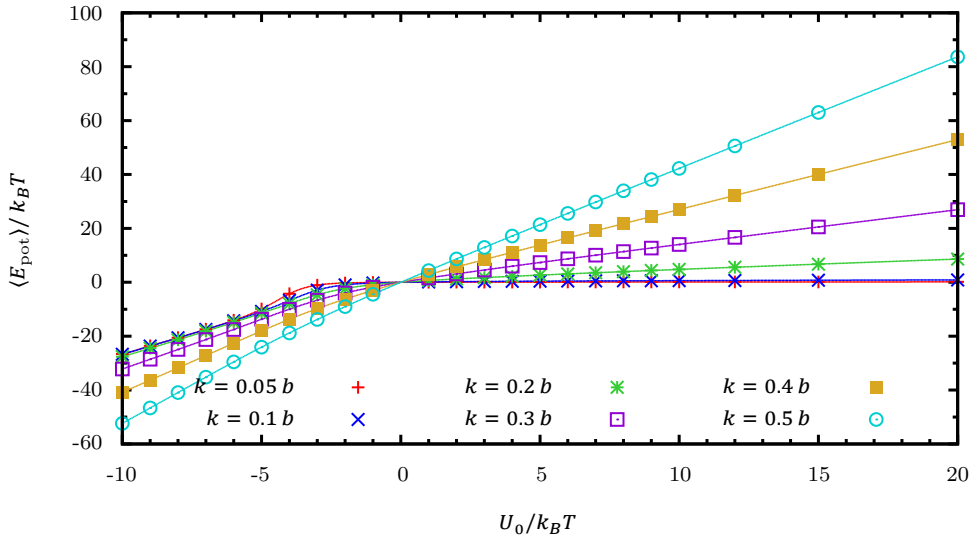

Figure 9. The above figures show the potential strength U_0 dependency of **(a)** the relative diffusivities D/D_0 and **(b)** the mean potential energies $\langle E_{\text{pot}} \rangle$ of point particles, recorded at different ranges k. Hydrogel model 1, as described in section 2.1, was employed to obtain this data. The lines in **(a)** are included to guide the eye. In contrast, the lines in **(b)** are the result of numerical calculation of the mean potential energies $\langle E_{\text{pot}} \rangle$ (performed with the MATHEMATICA software using the built in function `NIntegrate`) and the points were recorded by use of BD simulation. The colors are according to the different ranges used, as indicated in the legend.

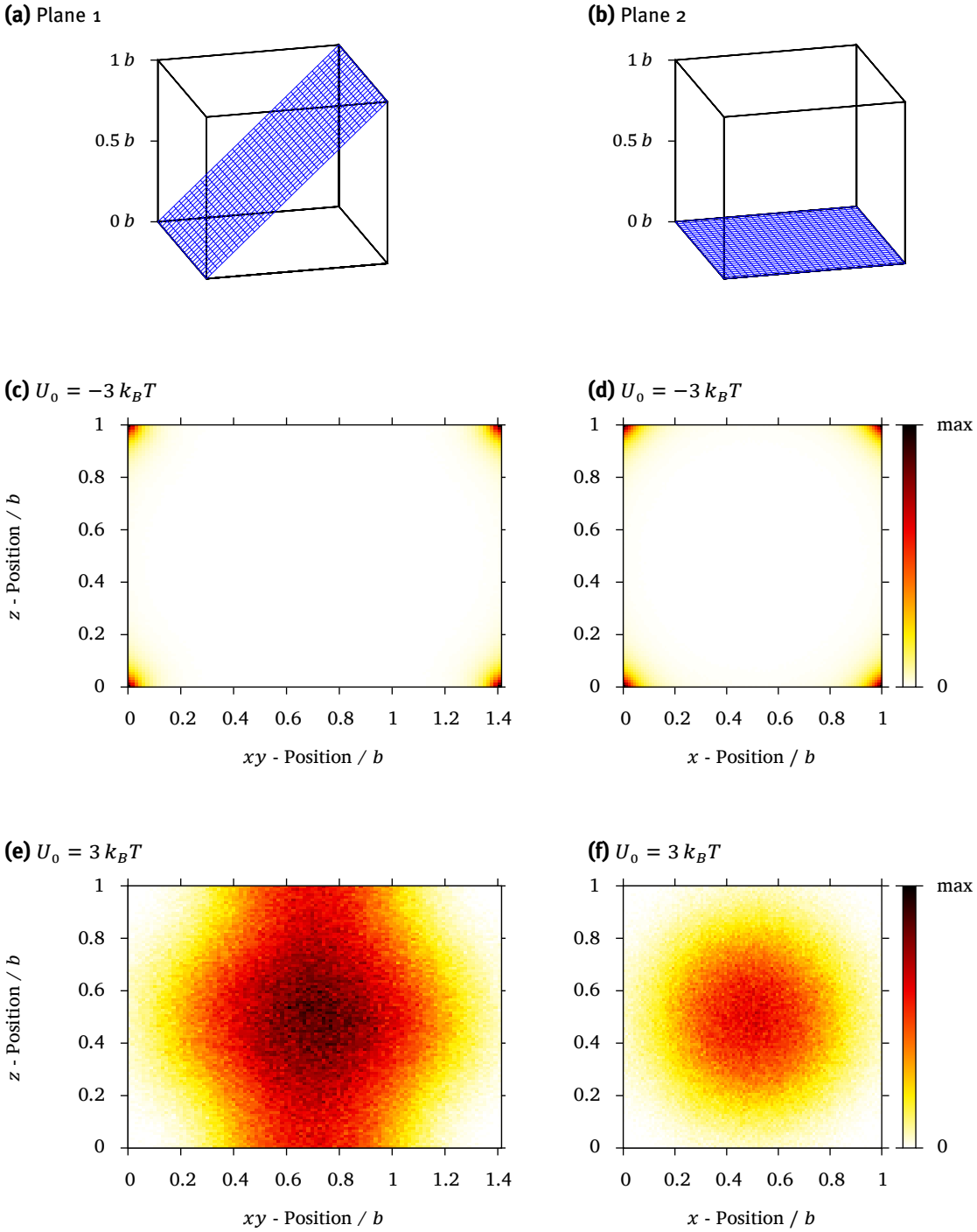

Figure 10. The probability of finding a point particle in certain areas of the simulation box is indicated by the color spectrum. The contour plots on the left (c, e) show the probabilities of finding the particle on *plane 1*, depicted at the top left (a) and the figures on the right (d, f), the probabilities of finding the particle on *plane 2*, depicted on the top right (b). The interaction range for all four plots is $k = 0.2\,b$. For the two middle figures (c, d) a repulsive and for the two bottom figures (e, f) an attractive interaction potential is used.

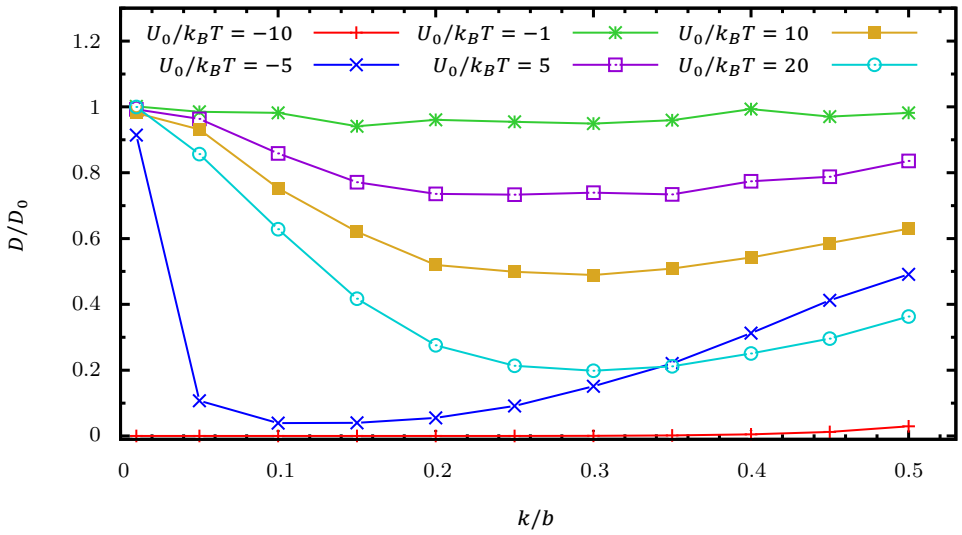

Figure 11. The relative diffusivity D/D_0 plotted over the interaction range k for point particles at a polymer distance $d = 0$, i.e. using model 1. The different colors of the data indicates simulations at different potentials strengths U_0, where $U_0 < 0$ indicates attractive and $U_0 > 0$ indicates repulsive interaction potentials. The lines are included to guide the eye. D_0 is the free diffusion coefficient.

step to be recorded and has been thus neglected. The minimum in the attractive case is partly due to the shape of the potential barrier between two sticking sites, which is presented for a generic potential strength in fig. 12b. The height of this potential barrier for attractive potentials depending on the interaction range k is presented in fig. 12d. For increasing interaction ranges k the potential barrier decreases, which is in line with an increase in diffusivity for ranges $k > 0.2\,b$, but the maximum potential difference lies at $k = 0$, therefore, the shape of the potential difference $\Delta U^{\mathrm{i}}_{\mathrm{ec}}$ alone cannot explain the minimum at $k = 0.15\,b$ for $U_0 = -5\,k_BT$. The reason the diffusivity increases for ranges $k < 0.15\,b$ is that the particle spends a lot of time outside the range of the interaction potential, where it can diffuse freely. "The stronger the potential, the stronger the effect of changing the range" holds for both the attractive and the repulsive regime. Nevertheless, changing the interaction range k seems to have a stronger impact on the diffusivity at attractive interaction potentials ($U_0 < 0$), than at repulsive interaction potentials ($U_0 > 0$). To see this one can, for example, compare the lines for $U_0 = \pm 5\,k_BT$ in fig. 11. This is a noteworthy trend that has also been observed above, in the discussion of fig. 9a.

Figure 9b includes a test of plausibility of the simulation results. The lines in this figure were obtained by numerical integration of the expression in eq. (11). The numerical integration was performed with the MATHEMATICA software using the built

(a) $U^{\mathrm{i}}(\vec{r})$ along the middle axis.

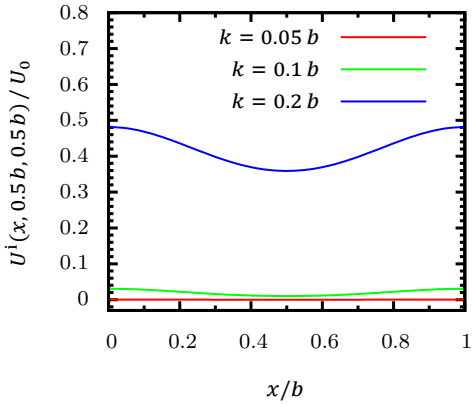

(b) $U^{\mathrm{i}}(\vec{r})$ along the edge.

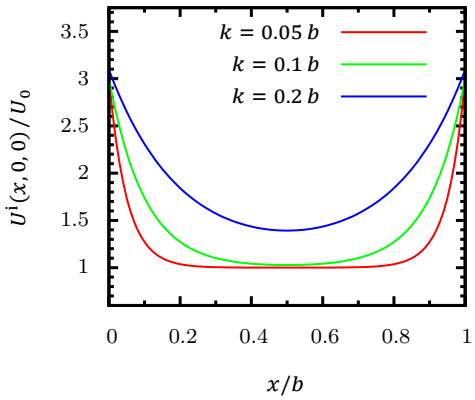

(c) Center-side energy difference.

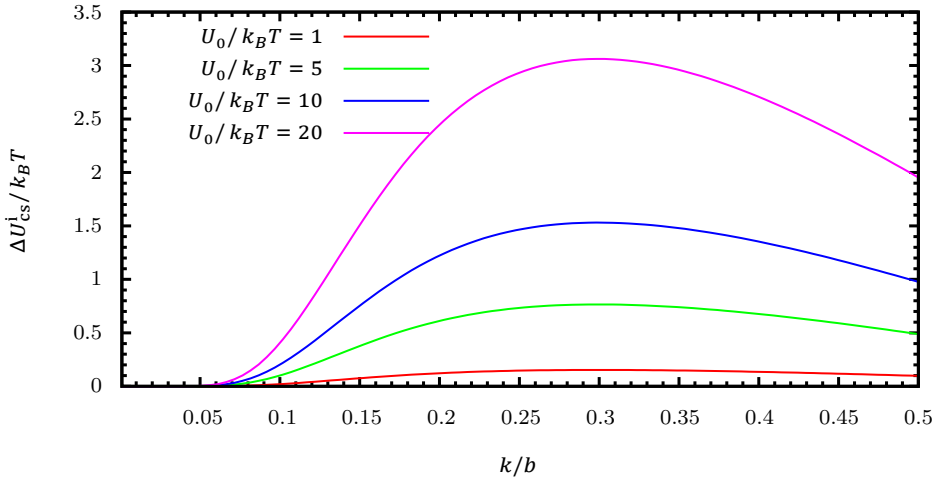

(d) Edge-corner energy difference.

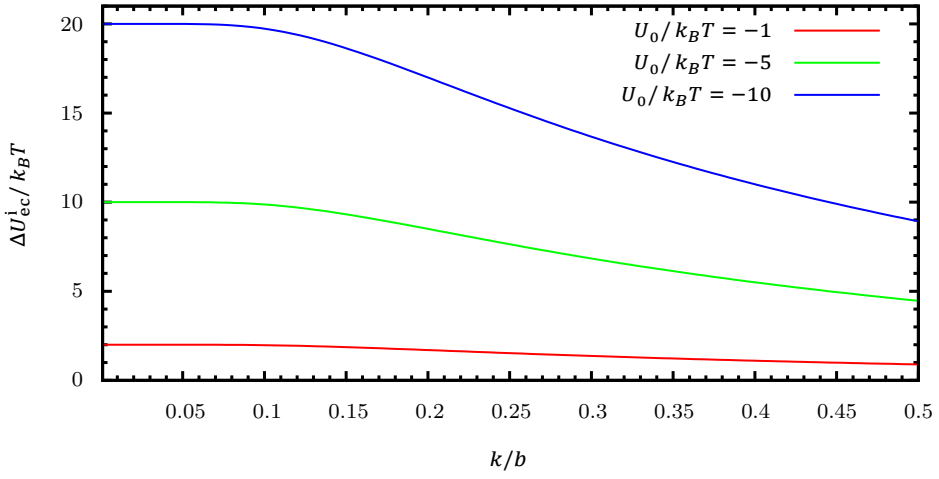

Figure 12. We present the shape of the interaction potential $U^{\mathrm{i}}(\vec{r})/U_0$ **(a)** along the middle axis of the simulation box and **(b)** along the edge of the simulation box. Note, that the interaction potential is normalized with the potential strength U_0 to indicate the relative shape of the curve. The middle and bottom figure show the interaction potential differences $\Delta U^{\mathrm{i}}_{\nu}$ **(c)** between the center and the side of the simulation box, indicated by an index $\nu = cs$, and the interaction potential difference between **(d)** the corner and the middle of the edge of the simulation box, indicated by an index $\nu = ec$. These potential differences are proportional to the depths of the minima in **(b)** and **(a)**. Here, they are presented in dependence of the interaction range k for different potential strengths U_0. The $U^{\mathrm{i}}(\vec{r})$ values are the analytic solutions of eq. (19).

in function `NIntegrate`. Evidently, the numerical results fit the simulation results very well. This shows, that the simulation results in fact obey Maxwell-Boltzmann statistics, as explained in section 2.5.

Model 2 and 3

The effect of modifying the potential or spatially separating the rods at the intersections by a nodal displacement d is presented in fig. 13. The $d = 0\,b$ data corresponds to model 1. In comparison, the model 2 data ($d < 0$) and model 3 data show larger relative diffusivities D/D_0 for attractive interaction potentials ($U_0 < 0$). For repulsive interaction potentials ($U_0 > 0$), the shapes of the curves are very similar. Thus, both methods successfully reduce the sticking effect but have no great influence on the trapping effect. Increasing the interaction range k reduces the "anti-sticking" effect of displacing the polymer chains relative to each other, which can be seen when comparing the positions of the green $d = 0.2\,b$ data in figures 13 a to c. Here, one can nicely see how the diffusivity is more sensitive to an increase in attractive potential strength for a larger range $k = 0.2\,b$ than for smaller ranges $0.1\,b$ and $0.05\,b$. Modifying the potential as described in section 2.1 - Model 3 reduces the sticking effect most effectively at at small attractive potential strengths U_0. It does not show a strong interaction range dependency, similar to the hydrogel model 1 data. The shape of the model 3 curves in the attractive regime is different than that of the model 1 and model 2 curves. This indicates that the potential modification not only decreases the sticking effect, but also changes the quality of the diffusive behavior. Hence, model 2 would be a more suitable approach to decrease the sticking effect in our hydrogel model.

The general behavior of the simulation does not change through either modification. A sticking and a comparatively weaker trapping effect can always be observed. Thus, as we observe agreement in trend between all three models and since we want to focus on a generic and simple coarse-grained model, we will use model 1 for further discussions including steric interactions.

4.3 Finite-size Particles

Including steric effects (c.f. section 2.3) has a strong impact on the diffusive behavior. This can be observed, for example, in fig. 14 where the interaction strength is put to $U_0 = 0$, and steric hindrance is included by use of the three different methods introduced in section 2.3. All three methods, truncated LJ and hardcore potential 1 and 2, appear to produce very similar results, i.e. the relative diffusivity D/D_0 approaches

(a) $k = 0.05\,b$

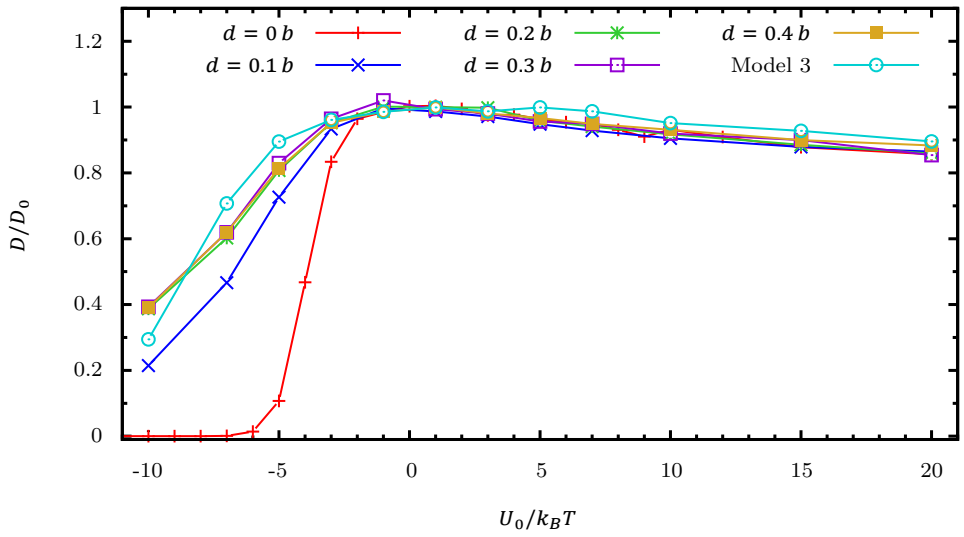

(b) $k = 0.1\,b$

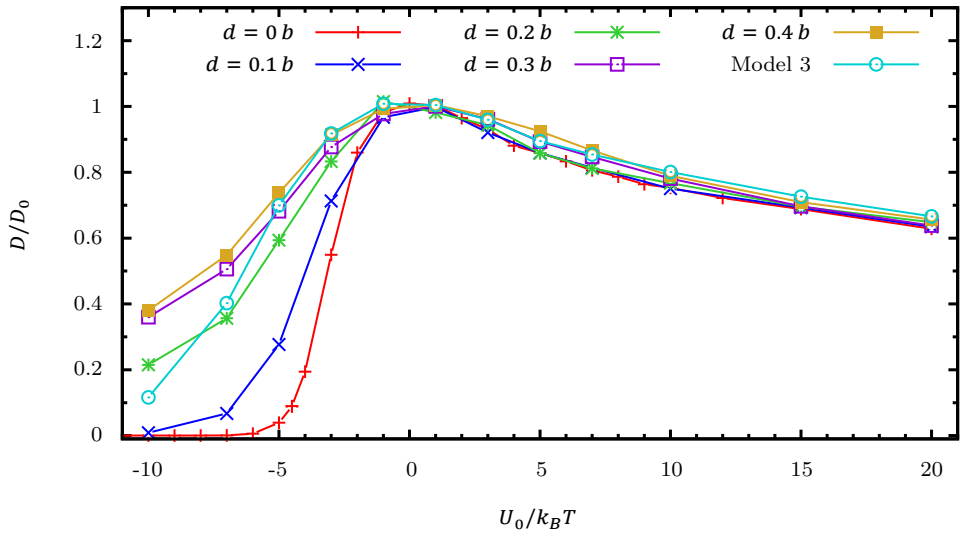

(c) $k = 0.2\,b$

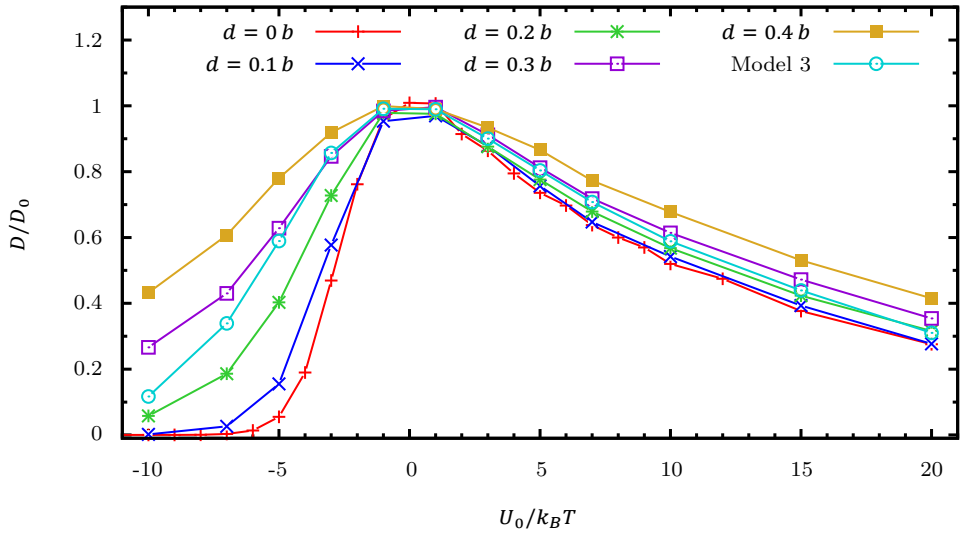

Figure 13. Comparison between the three hydrogel models described in section 2.1, for different ranges **(a)** $k = 0.05\,b$, **(b)** $k = 0.1\,b$ and **(c)** $k = 0.2\,b$. The lines are included to guide the eye. D_0 is the free diffusion coefficient.

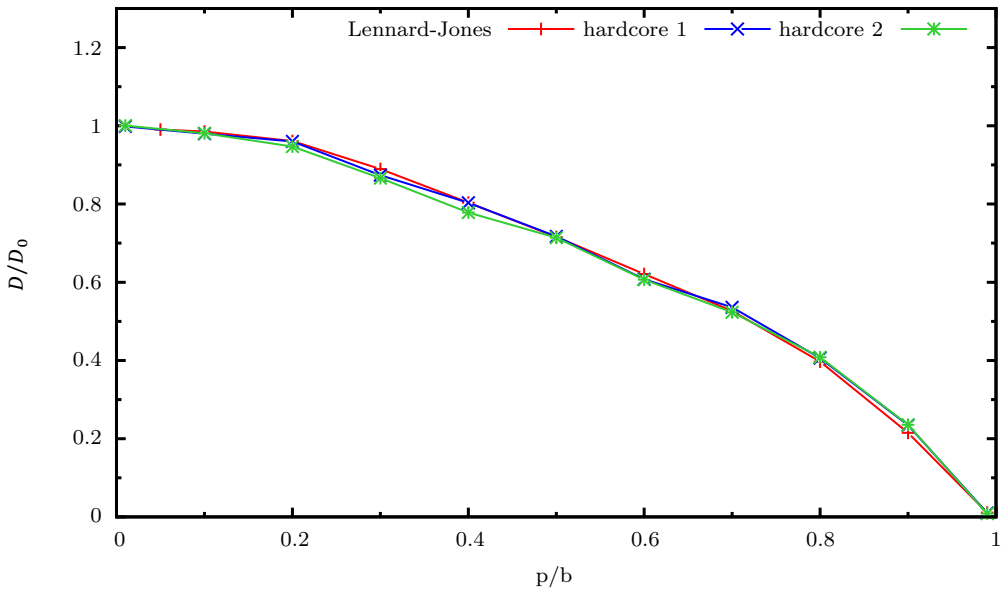

Figure 14. Comparison of the purely steric hindrance for the three different methods of including steric effects, i.e. truncated LJ, hardcore 1 and hardcore 2, as introduced in section 2.3. The lines are included to guide the eye. D_0 is the free diffusion coefficient.

unity as the particle diameter p approaches zero. For p approaching the width of the simulation box b, the relative diffusivity approaches 0, since the particle eventually cannot cross between lattice cells anymore, due to steric hindrance. The data is also in qualitative agreement to the data by Netz and Dorfmüller, who simulated a similar cubic geometry and a spherical tracer without electrostatic or hydrodynamic interactions [22].

The effect of a combination of interaction potential U^{i} and steric interaction U^{s} is presented in figs. 15b, 16a and 16b by use of the truncated LJ potential and hardcore potential 1 and 2, respectively. Comparing those three figures one can see at first glance, that all three methods of introducing steric interaction qualitatively produce the same results. Hence, in all following data presented in this work only the truncated LJ potential will be used.

The diffusivity is highly dependent on the particle diameter p. Larger particles experience much less of a sticking effect than smaller particles, since due to their larger size, they cannot get so close to the polymer chains, i.e. the potential minima in the attractive regime. This becomes obvious when looking at the contour plots in figs. 17a and 17b for finite-size particles of diameter $p = 0.3\,b$. In the attractive regime at $U_0 = -3\,k_BT$ the particles are most of the time in the corners of the box, but due to steric interaction, they can not get closer than $p/2 = 1.5\,b$ to the edges,

which results in the white spaces in the corners and sides of the contour plots. This is in contrast to point particles, which can travel infinitely close to the potential minima in the corners of the simulation box, as can be observed in fig. 10. Thus, they spend much more time in the corners of the simulation box and, correspondingly, experience a stronger sticking effect than finite-size particles. Figure 15 also reveals that at small interaction range $k = 0.05\,b$, larger particles of diameter $p > 0.2\,b$ are only affected very little by changes in the potential strength U_0 and their diffusion is only hindered by steric effects, which are stronger for larger particles than for smaller particles, as one would expect intuitively. In the investigated regime of $U_0 = -20$ to $20\,k_BT$, only small particles of size $p = 0.1\,b$ experience strong sticking. At a larger interaction range of $k = 0.2\,b$ in the attractive regime (c.f. fig. 15c) larger particles also are less affected than smaller ones. This is a noteworthy effect, since it implies that an attractive interaction potential actually immobilizes smaller particles more efficiently than larger particles in this model.

Interestingly, in the repulsive regime the size effect seems to vanish towards larger potential strengths U_0 for particles with a diameter between 0.1 and $0.5\,b$. This is due to the particles being "trapped" in the center of the box for most of the time, as can be observed in the contour plots in figs. 17c and 17d. In the center of the box steric effects barely come into play, as long as the width p of the particle is not close to the box size b. This is the reason why the difference to the point particle contour plots (c.f. figs. 10c and 10d) is less pronounced than in the attractive regime (negative U_0). Nevertheless, the excluded volume effect in the form of the white spaces near the edges of the simulation box is also clearly visible, here.

Figure 15c shows that larger particles with a diameter $p = 0.9\,b$ experience an increase in diffusivity towards stronger attractive potentials. This effect occurs, since an attractive potential between polymer chains and particle counteracts the repulsive steric interaction, e.g. the truncated LJ potential, leading to a lowering of the total potential barrier which the particle has to cross between adjacent lattice boxes.

One can furthermore observe that particles with smaller diameter, e.g. $p = 0.1\,b$, are more effectively hindered than larger ones, e.g. with a diameter of $p = 0.5\,b$. This is because they can get closer to potential minima in the corners of the simulation box or, in other words, because larger particles experience a more homogeneous potential than smaller ones. To examine this size-effect more closely we show the dependency of the particle diffusivity D/D_0 on the particle size p in fig. 18 for different combinations of interaction range k and potential strength U_0. One can see that, in the repulsive case, i.e. at positive $U_0 = 10,\ 20\,k_BT$, the relative diffusivity decreases

(a) $k = 0.05\,b$

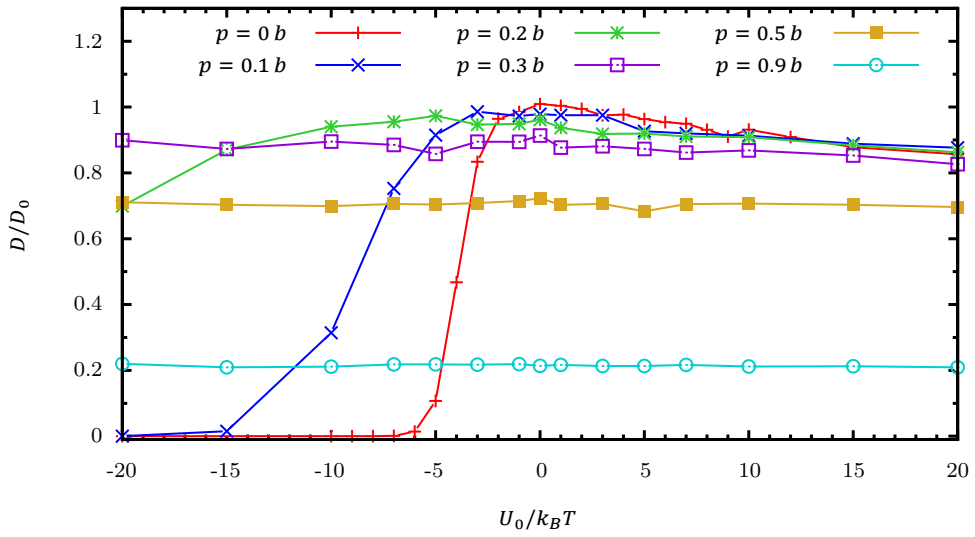

(b) $k = 0.1\,b$

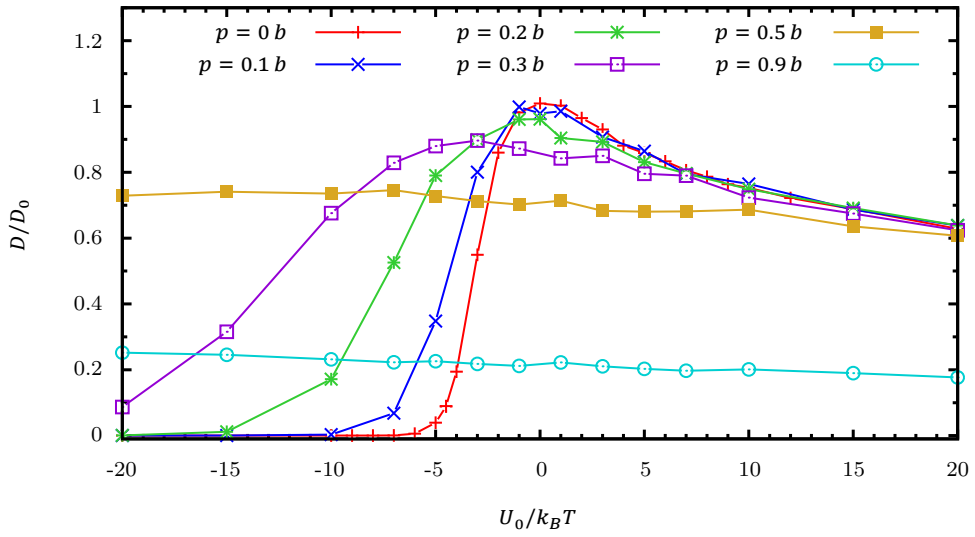

(c) $k = 0.2\,b$

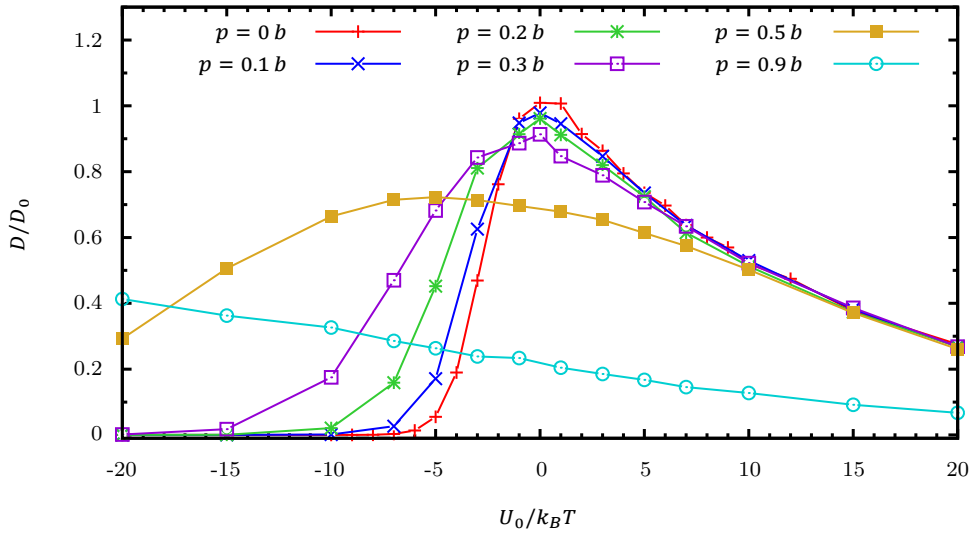

Figure 15. Comparison of the simulation results including steric interactions in the form of a truncated LJ potential for different effective particle sizes p (c.f. eq. (4)) and for different ranges of **(a)** $k = 0.05\,b$, **(b)** $k = 0.1\,b$ and **(c)** $k = 0.2\,b$. The lines are included to guide the eye. D_0 is the free diffusion coefficient.

(a) Hardcore potential version 1.

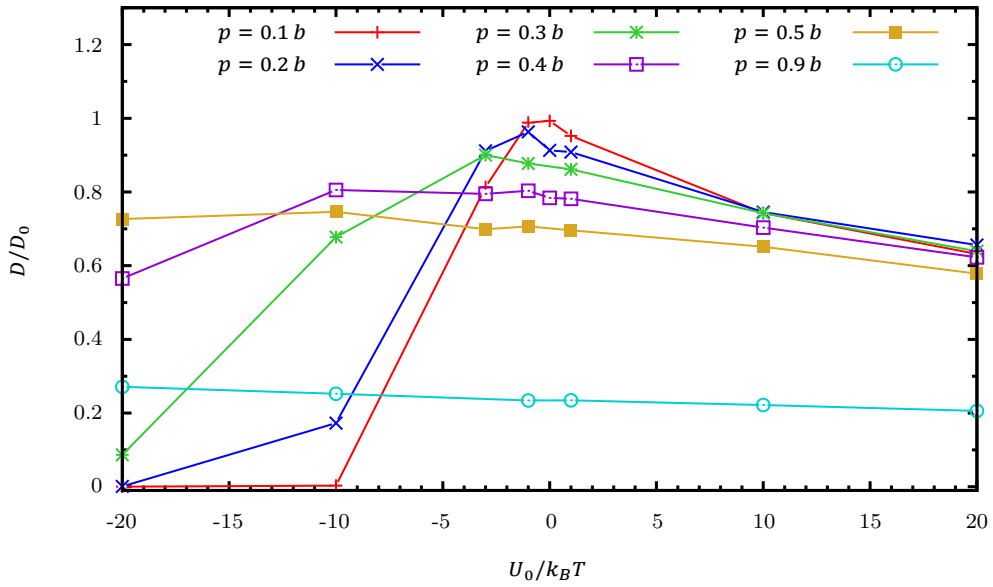

(b) Hardcore potential version 2.

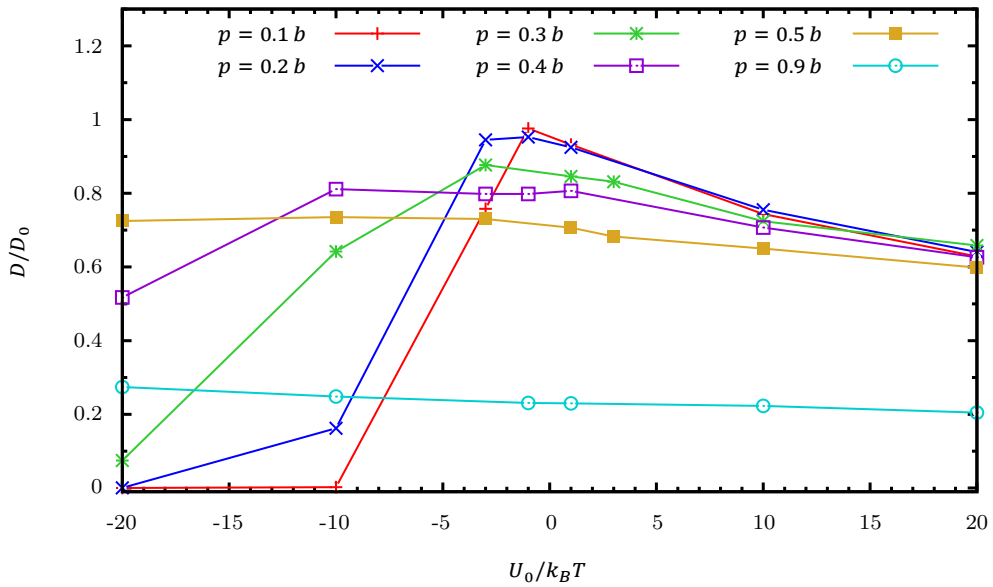

Figure 16. Comparison of the two different hardcore potentials introduced in section 2.3 at a range of $k = 0.1\,b$. The data in figure **(a)** has been obtained using the hardcore potential version 1, the data in figure **(b)** using hardcore potential version 2. The lines are included to guide the eye. D_0 is the free diffusion coefficient.

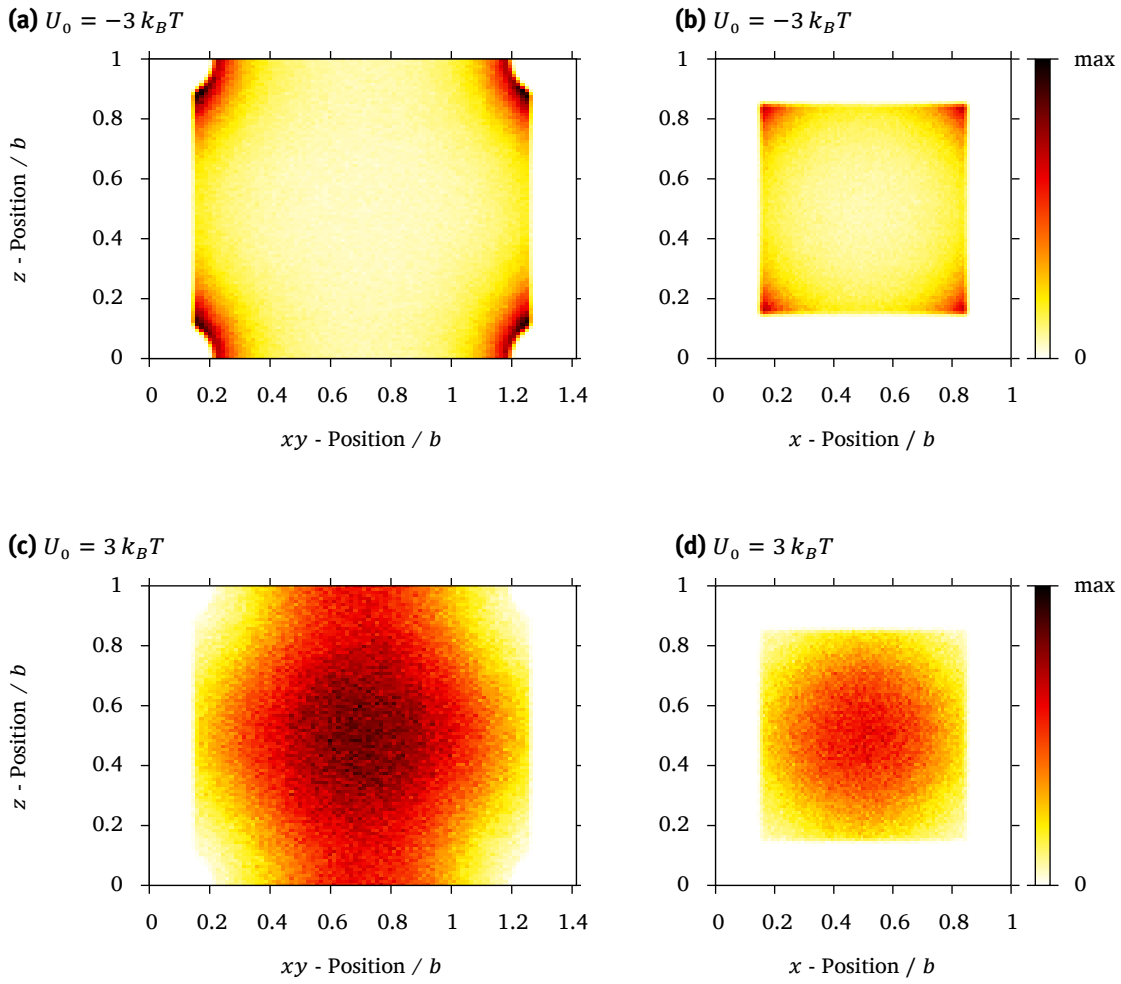

Figure 17. The probability of finding a finite-size particle ($p = 0.3\,b$) in certain areas of the simulation box is indicated by the color spectrum. The depicted areas are plane 1 and plane 2 as shown in fig. 10. The steric interaction is included via the truncated LJ potential. The figures on the left (a, c) show the probabilities of finding the particle on plane 1 and the figures on the right (b, d) the probabilities of finding the particle on plane 2. The range for all four plots is $k = 0.2\,b$. The two middle figures (a, b) / bottom figures (c, d) show the case of attractive/ repulsive interaction with the potential strength set to $U_0 = -3\,k_BT$ / $U_0 = 3\,k_BT$.

monotonously towards larger particle diameters p, approaching a value close to zero for $p = b$. For negative $U_0 = -3, -10, -20\,k_BT$ on the other hand, increasing the particle size at a constant range initially leads to an increase in diffusivity D/D_0 up to a maximum at an intermediate p, beyond which the relative diffusivity decreases again approaching a value close to zero for $p = b$, similar to the repulsive case. This behavior occurs at all three depicted ranges $k = 0.05$, 0.1 and $0.2\,b$, but less pronounced at smaller ranges than at a larger ranges. The maximum occurs, since for increasing particle diameters the sticking effect due to an attractive interaction potential decreases, such that beyond a certain particle size the hindrance effect of the steric interaction becomes dominant and the diffusivity decreases again for increasing particle sizes. At positive $U_0 = 10, 20\,k_BT$ both the total interaction potential U^{i} and the total LJ potentials U^{s} are repulsive and the particle experiences trapping in the center of the simulation box. This trapping is the reason that the relative diffusivity D/D_0 remains constant at small particle sizes p, because small trapped particles do not "feel" the truncated LJ potential (c.f. eq. (4)). This difference in the behavior for attractive and repulsive interaction potentials is an interesting peculiarity of the model and will be further discussed in section 5, when the model is compared to experimental findings.

In fig. 19 we compare the effect of changing the range for different particle sizes in the attractive regime at $U_0 = -10k_BT$ and in the repulsive regime at $U_0 = 10k_BT$. The larger the particle, the less affected is its diffusivity D by changes of k. This goes for both cases, attractive and repulsive. At smaller ranges the particles are predominantly hindered by steric interactions, thus their relative diffusivities D/D_0 approach a maximal value for decreasing k, which corresponds to the purely steric hindrance. This region of predominantly steric hindrance is particularly well visible in the $U_0 = -10k_BT$ plot in fig. 19a, where one can see a relatively clear drop in the D/D_0 values of the $p = 1,\ 2$ and $3\,b$ curves, which lies at around $k = p/3$. In both plots the diffusivities increase again for most particle sizes, at interaction ranges larger than around $k \geq 0.2\,b$ for $U_0 = -10\,k_BT$ and around $k \geq 0.3\,b$ for $U_0 = 10\,k_BT$. This is due to the potential becoming relatively homogeneous inside the unit cell, as discussed for point particles. For large particles of diameter $p = 0.9\,b$ this is not the case and the curve has a maximum at around $k = 0.3\,b$. The reason for this is the same as mentioned earlier, namely, that an attractive potential between polymer chains and particle counteracts the repulsive steric interactions of the polymer chains, which can lead to an increase in diffusivity. The maximum is also due to the homogeneity of the total interaction potentials inside the simulation box at large ranges k.

(a) $k = 0.05\,b$

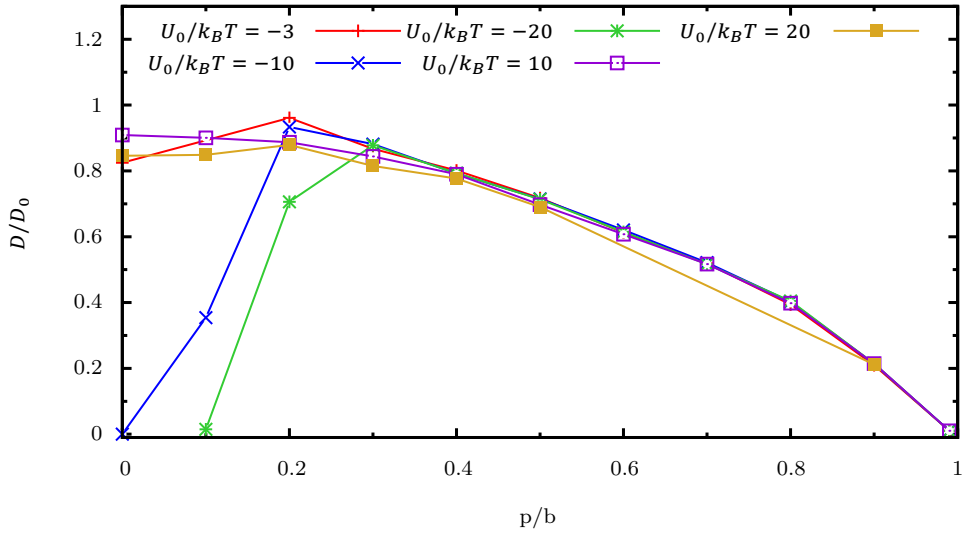

(b) $k = 0.1\,b$

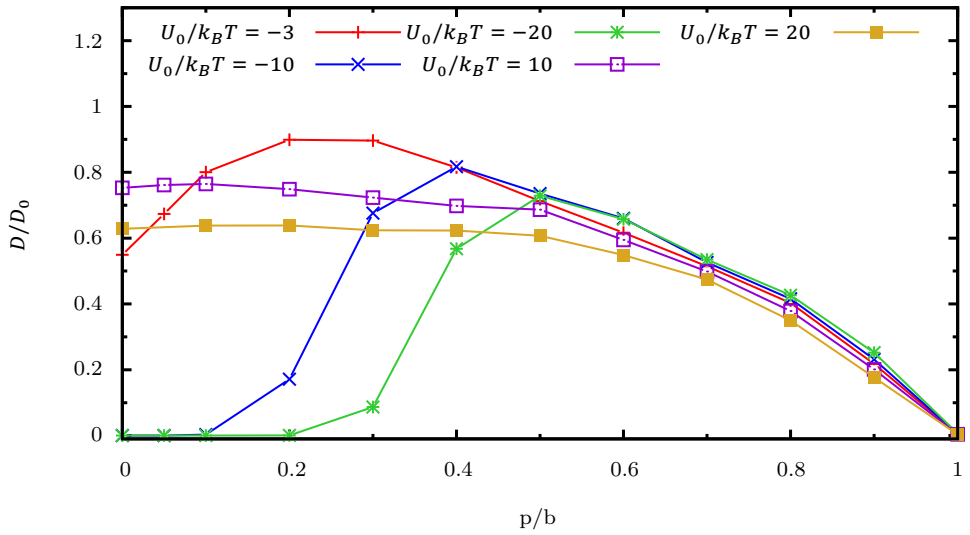

(c) $k = 0.2\,b$

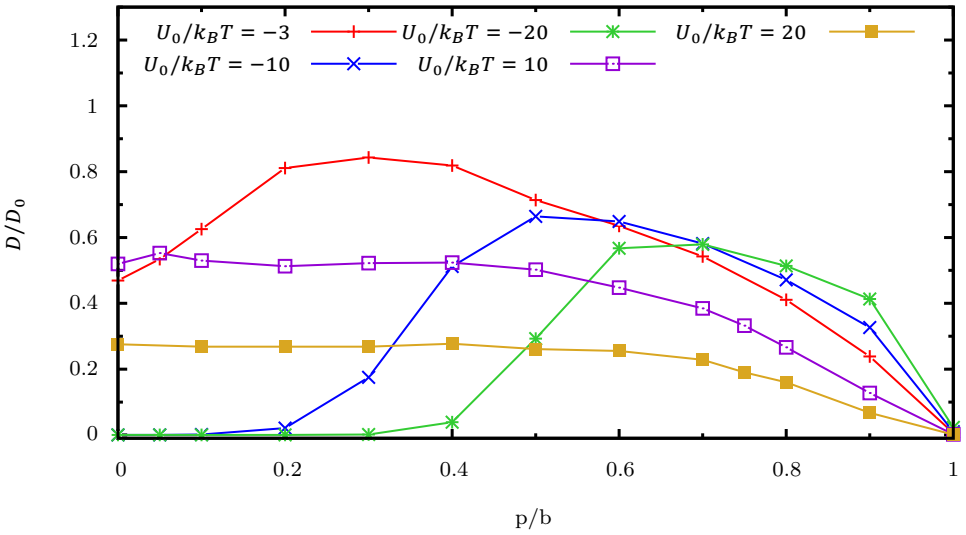

Figure 18. The effect of varying the particle size p for different potential strengths U_0 and interaction ranges **(a)** $k = 0.05\,b$, **(b)** $k = 0.1\,b$ and **(c)** $k = 0.2\,b$. The lines are included to guide the eye. D_0 is the free diffusion coefficient.

(a) $U_0 = -10\,k_BT$

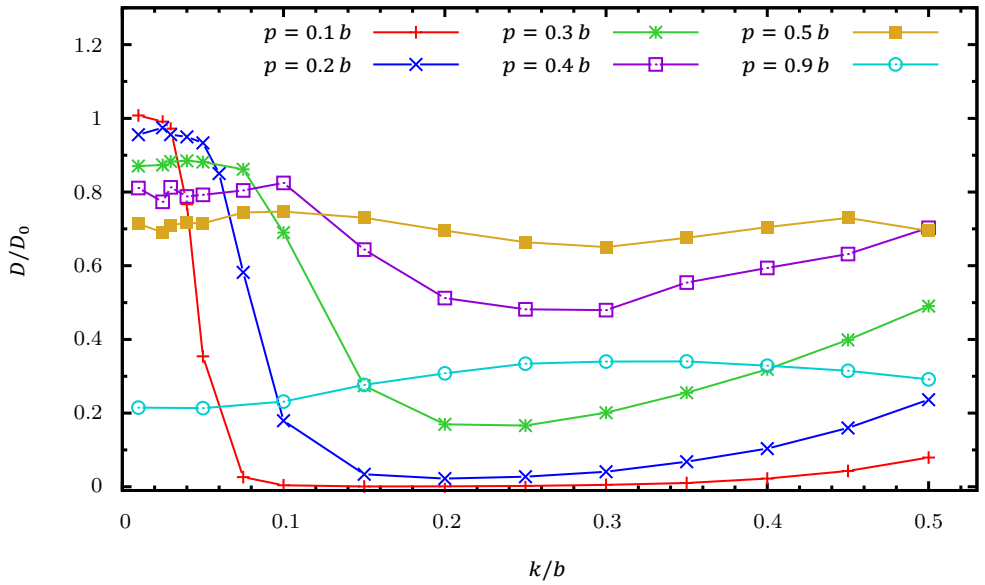

(b) $U_0 = 10\,k_BT$

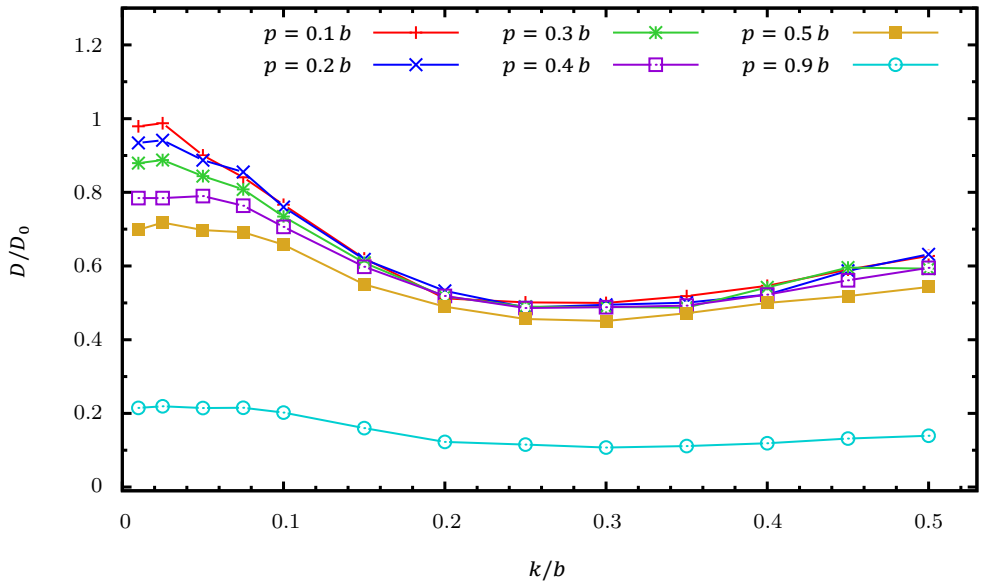

Figure 19. Comparison of how changing the range k affects the diffusivity of differently sized spherical particles at a potential strength **(a)** $U_0 = -10\,k_BT$ (attractive interaction) and **(b)** $10\,k_BT$ (repulsive interaction). Steric interactions are included in the form of the truncated LJ potential. Note that decreasing the range k corresponds to increasing the salt concentration in the hydrogel. The lines are included to guide the eye. D_0 is the free diffusion coefficient.

4.4 Random Charge Model

The simulation data for randomly attractive or repulsive simulation box edges, as introduced in section 2.2, will be presented in a fashion similar to the results for hydrogel model 1. Hence, the case of point particles will be presented at first and subsequently finite-size particles will be discussed. Figure 20a shows the dependency of point particle diffusivity on the potential strengths U_0 for different interaction ranges k. The observed data looks qualitatively similar to the corresponding data for charged hydrogels of model 1 type, i.e. for increasing potential strengths the particle experiences decreasing long-time diffusivity. This can be seen by comparing the shape of the curves in fig. 20a to the shape of the curves going from $U_0 = 0$ to increasing negative U_0, but also to increasing positive U_0, e.g. at a range of $k = 0.3\,b$ in fig. 9a. In the latter case the decrease in diffusivity for increasing U_0 occurs slower, but the shape of the data curves is qualitatively similar. A closer comparison of fig. 20a and fig. 9a reveals that the random potential model data is similar to the case of purely attractive interaction, since almost equivalently the relative diffusivity gets close to zero for all three ranges $k = 0.05,\ 0.1,\ 0.2\,b$ at around $U_0 = 7\,k_BT$. In the purely repulsive case this is not observed in the investigated range of $U_0 \leq 20\,k_BT$.

The observed long-time diffusive behavior of point particles in a random potential type hydrogel implies, that although the net charge of the hydrogel ist zero, charged particles still experience increasingly hindered diffusivity for increasing surface charges. Whether it is trapping or sticking that causes this immoblization can be readily answered by a close look at fig. 20b, which shows the mean potential energies $\langle E_{\text{pot}} \rangle$ of the point particles, recorded at different interaction ranges k and potential strengths U_0. One immediatly sees that the mean potential energy of the particle is always negative. Hence, it tends to spend more time near attractive rods than near repulsive ones. For large potential strengths the absolute mean potential energy of the particle is almost three times the full interaction potentials strength $-U_0$ of a single attractive rod. This indicates that the particle stays almost all the time in the corners of the simulation box, i.e. it experiences sticking with a potential energy of close to $-3\,U_0$. This is confirmed by the contour plots in figs. 21c and 21d where a red and dark coloring indicates a high probability density of finding the particle in the corners of the simulation box, similar to the contour plots for point particles in an attractive potential shown in figs. 10c and 10d but with a slightly less pronounced probability maximum in the corners.

Figure 22 shows the relative diffusivity D/D_0 in dependence of the interaction range

(a) Relative diffusivities

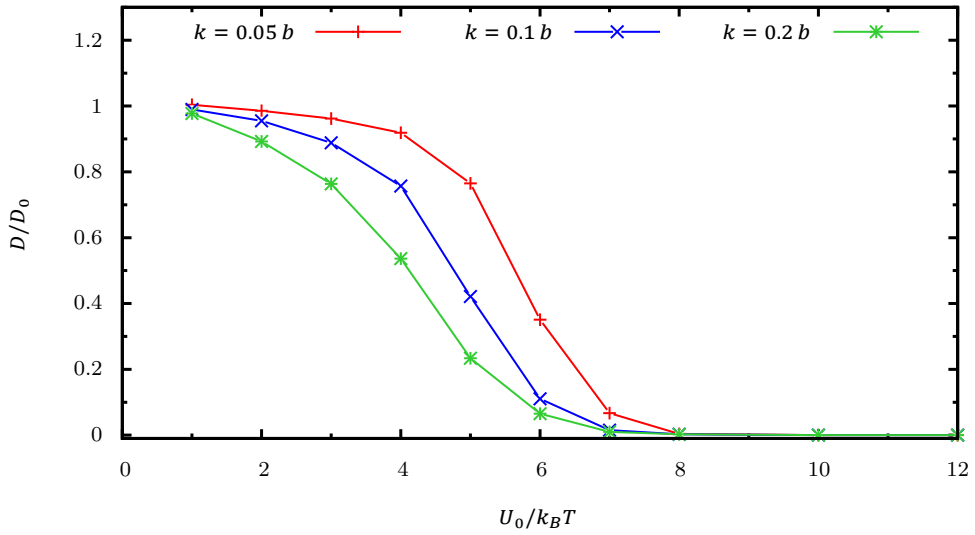

(b) Mean potential energies

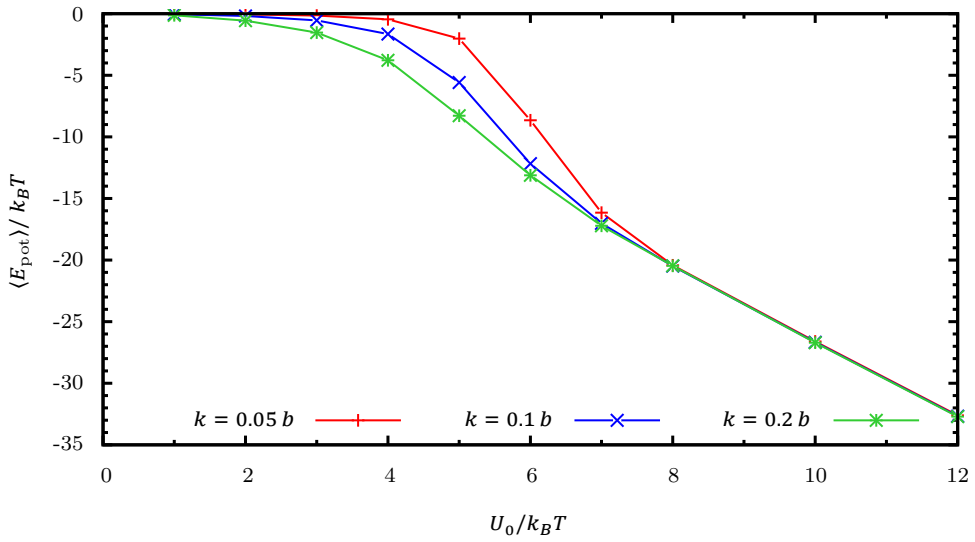

Figure 20. The above figures show the potential strength U_0 dependency of **(a)** the relative diffusivities D/D_0 and **(b)** the mean potential energies $\langle E_{\mathrm{pot}}\rangle$ of point particles, recorded at different interaction ranges k. The random charge model hydrogel as described in section 2.2 has been used to obtain this data. The lines are included to guide the eye.

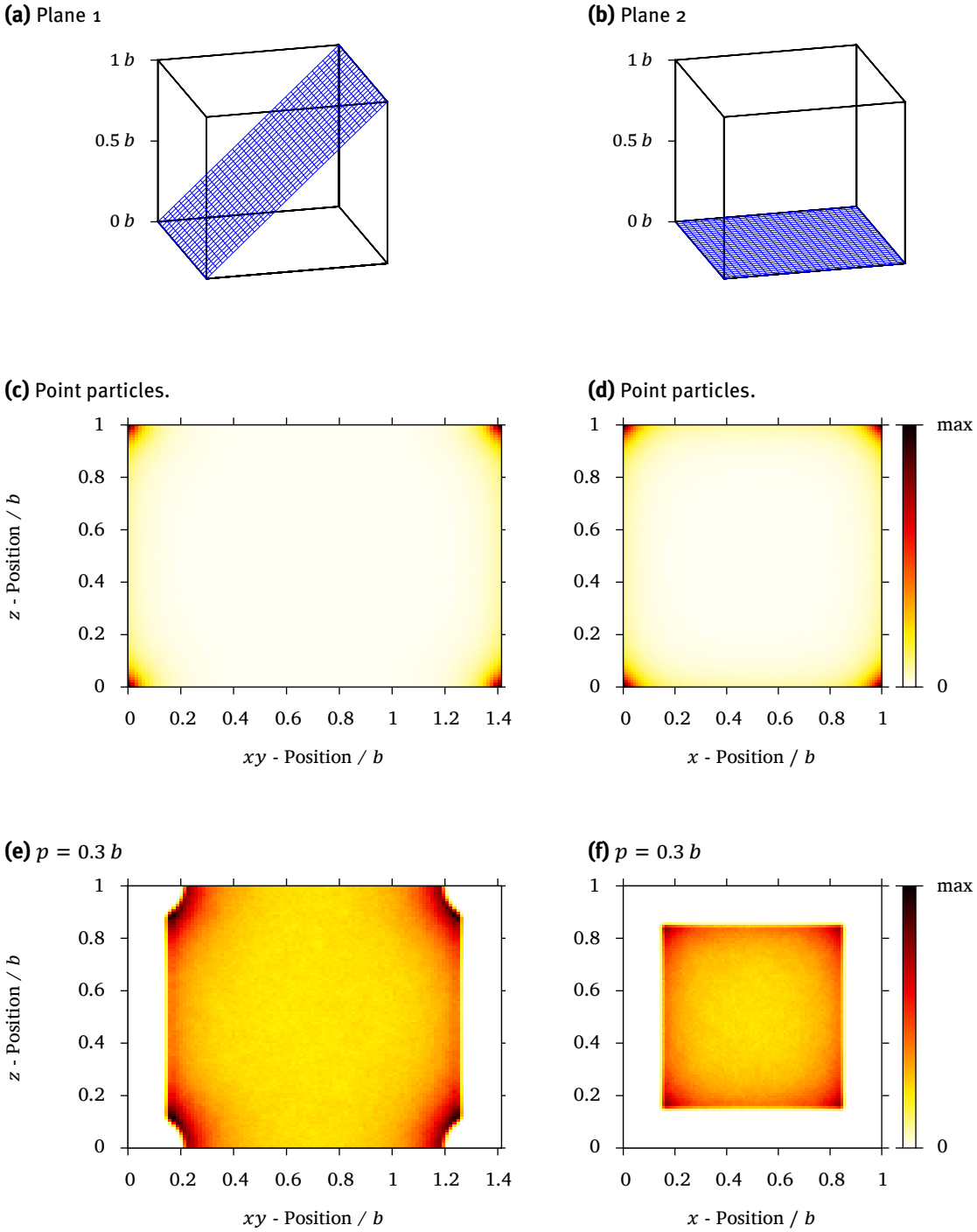

Figure 21. The probability of finding a point particle (c, d) and a finite-size particle of width $p = 0.3\,b$ (e, f) in certain areas of the simulation box is indicated by the color spectrum. The simulations were performed in a random charge model hydrogel with the potential strength randomly set to $U_0 = \pm 3\,k_B T$. The contour plots on the left (c, e) show the probabilities of finding the particle in *plane 1*, depicted in (a). The contour plots on the right (d, f) show the probabilities of finding the particle in *plane 2*, depicted in (b). The interaction range for all four plots is $k = 0.2\,b$.

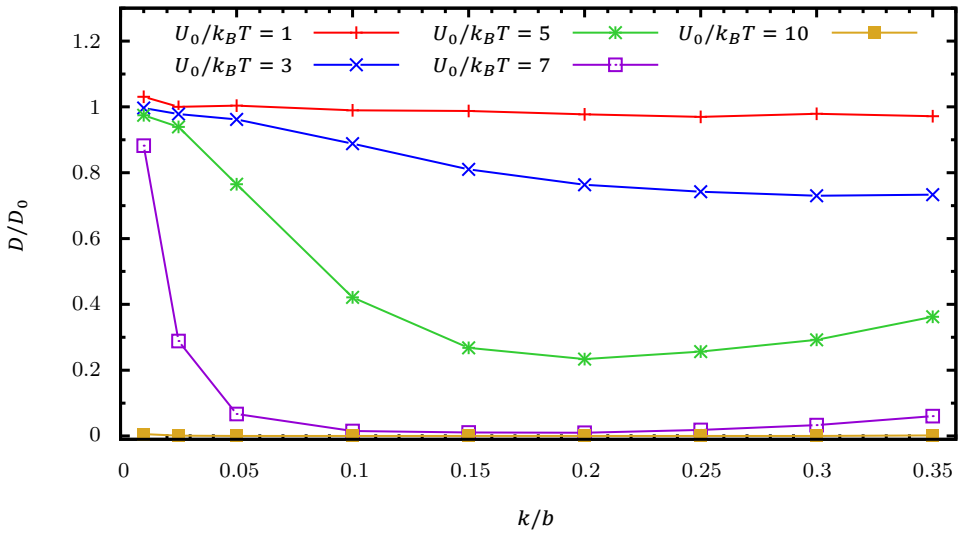

Figure 22. The relative diffusivities D/D_0 of point particles in a simulated random charge model hydrogel in dependence of the interaction range k, obtained at varying potentials strength U_0. The lines are included to guide the eye. D_0 is the free diffusion coefficient.

k at different potential strengths U_0. There is a minimum in the relative diffusivity at different ranges k, depending on the potential strength. Similar to the minimum in fig. 11, this occurs due to the different polymer chain potentials averaging out each other for long enough ranges, or, in other words, due to less well defined potential minima at the corners of the simulation box at longer ranges (c.f. section 4.2). Note that, as explained in section 3.2, only first order rods were included in the calculation of the total interaction potential, i.e. only the 12 nearest neighbor rods. This slightly reduces the comparability to hydrogel model 1 at ranges $k > 0.2\,b$, for which second order rods were also included. Nevertheless, the results are qualitatively the same, in that a minimal relative diffusivity occurs for a certain interaction range k.

Changing from point particles to finite size particles leads to similar effects as already observed for hydrogel model 1 in section 4.3. Namely, that larger particles experience less immobilization due to the interaction potential, than smaller particles. This can be readily observed in fig. 23, which shows the relative diffusivity D/D_0 in dependence of the interaction strength U_0 for particles of varying diameter p. At small interaction strengths the steric effect is dominant, therefore larger particles are less mobile than smaller ones, but for increasing U_0 smaller particles are immobilized much stronger than larger ones. One can interpret this, in the sense that smaller particles are more sensitive to changes in electrostatic interaction than larger particles. As in the case of point particles the dominant process causing immobiliza-

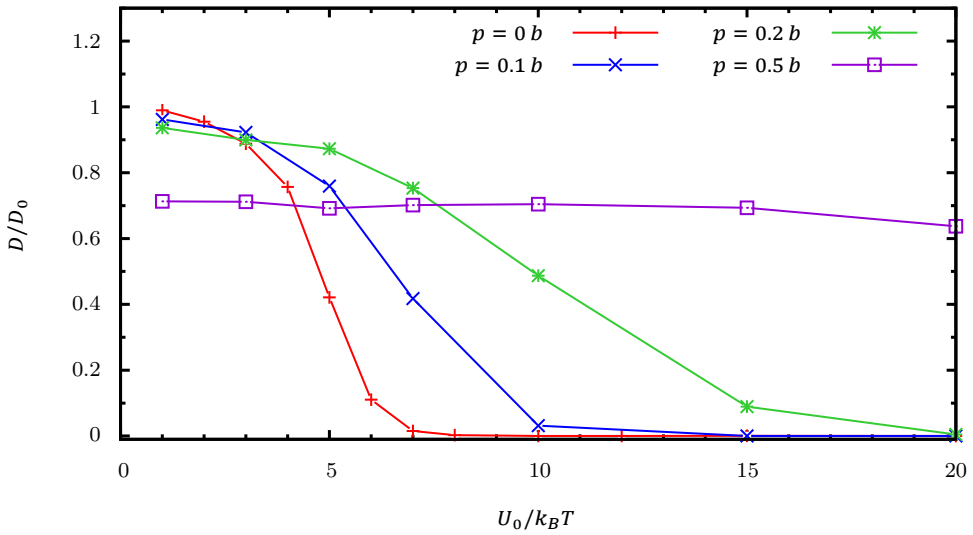

Figure 23. The relative diffusivities D/D_0 of finite-size particles of varying diameter p in a random charge model hydrogel plotted over the absolute potential strength U_0. A diameter of $p = 0\,b$ indicates data for point particles. The interaction range is set to $k = 0.1\,b$. The lines are included to guide the eye. D_0 is the free diffusion coefficient.

tion of finite-sized particles is sticking. This can be observed in the contour plots in fig. 21, which reveal that point particles, as well as finite-size particles, tend to be in the corners of the simulation box.

Figure 24 shows the particle diameter p dependency of the relative diffusivity D/D_0. Here, one can again see the similarity of the random potential model data to the purely attractive interaction hydrogel model 1 data shown in fig. 18. Small particles experience a dominant hindrance due to the interaction potential and larger particles experience a dominant steric hindrance, so particles of intermediate diameter are actually most mobile. This maximum in relative diffusivity shifts to larger particle diameters p and decreases in amplitude for increasing potential strength U_0.

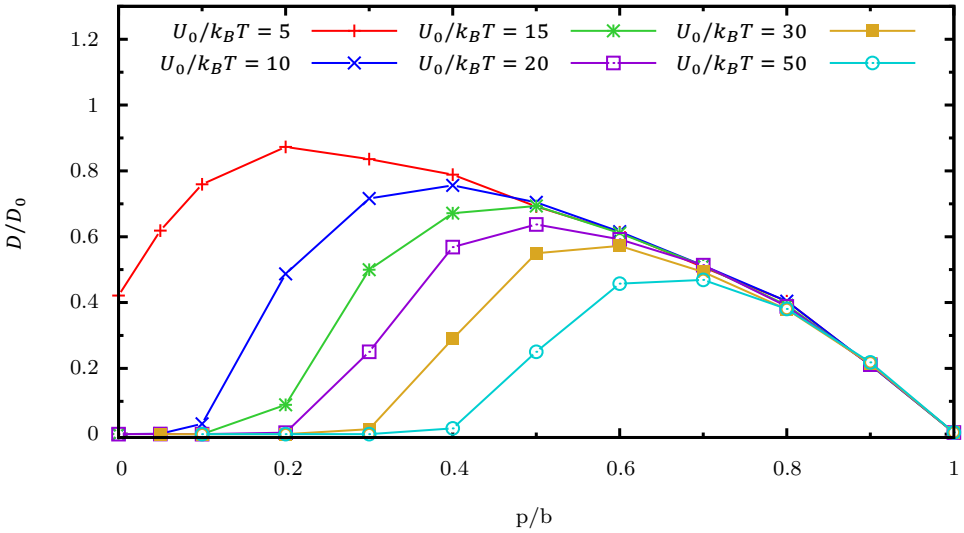

Figure 24. The effect of varying the particle size p for different potential strengths U_0 at an interaction range of $k = 0.1\,b$ for a random charge model hydrogel. The lines are included to guide the eye. D_0 is the free diffusion coefficient.

5 Comparison to Experiments

The ultimate test of our model is the comparison with experimental results. This serves as an indicator to gauge how helpful our model might be to understand physical processes and to make reasonable predictions about them. Thus, in this section we will present a careful comparison of our model with experimental findings for particle diffusion in hydrogels.

5.1 Qualitative Comparison

For a qualitative comparison of the results of the simulations to experimental findings it is useful to consider three different quantities, namely, changes in the salt concentration, in the polymer concentration and of the surface charge of the diffusing particle.

Polymer Concentration

For uncharged systems, i.e. neutral hydrogels, an increase in polymer concentration leads to a smaller mesh size [11], which corresponds to larger relative particle sizes p/b. Increasing p/b at $U_0 = 0$ leads to a decreasing diffusivity, as can be seen in fig. 25, which is by trend in accordance with experimental results [2, 9, 26, 32]. To enable a qualitative comparison to experimental data, our simulation data is presented as a function of diffusivity over polymer concentration in fig. 25. The polymer concentration is given in arbitrary units, to show the scaling for a linear increase in polymer concentration. It is assumed that the correlation length b is inversely proportional to the square root of the polymer concentration, as indicated in eq. (26). The concrete units depend on the chemistry of the hydrogel and the width of the tracer particle. In fig. 25, there appears to be a linear connection between polymer concentration and diffusivity. This is in accordance to experimental findings by [9], although other authors report a stretched exponential dependency on the polymer concentration [32, 33]. Thus, the simulation clearly reproduces the correct tendency, insofar that the diffusivity decreases with increasing polymer concentration, and the shape of the curves is in agreement with some experimental findings.

Another important aspect of the model is, that for particle sizes approaching the mesh size, i.e. larger polymer concentrations, the particles will eventually be entirely immobilized inside the hydrogel, due to stiffness of the polymer network. In a hydrogel, larger particles will diffuse with the bulk diffusivity of the hydrogel, which is

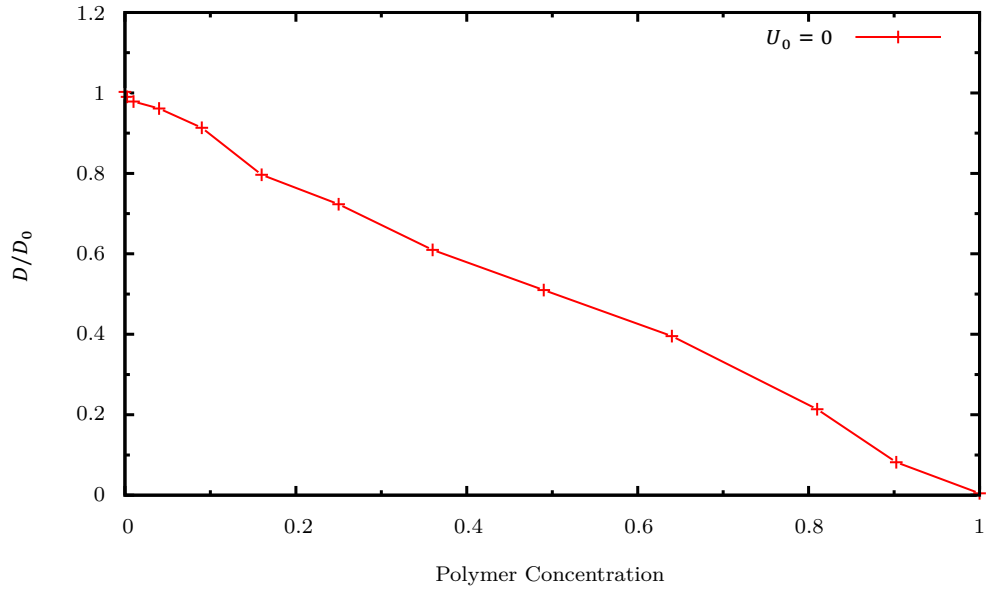

Figure 25. Effect of purely steric interactions (using the truncated LJ potential described in section 2.3) on the diffusivity of particles at different polymer concentrations. The polymer concentration is given in arbitrary units, only to show the scaling for a linear increase in polymer concentration, assuming the correlation length b is inversely proportional to the square root of the polymer concentration, as indicated in eq. (26). The concrete units depend on the chemistry of the hydrogel and the width of the tracer particle. The lines are included to guide the eye. D_0 is the free diffusion coefficient.

nonzero. Thus, in a real hydrogel, D/D_0 will approach a finite value different from zero.

Particle Surface Chemistry

In experiments, the method for decreasing the surface charge of polystyrene particles, which is related to the potential strength U_0, is usually PEGylation, as outlined for instance by Cu and Saltzmann [14] or Wang and coworkers [34]. Properly executed PEGylation effectively screens the surface potential of the test particles. For particles with a screened surface charge (e.g. PEGylated) or no surface charge, e.g. 1,2-dioleoyl-sn-glycero-3-phosphocholine (DOPC), the diffusion coefficient is in general higher and they are less affected by changes in salt concentration in comparison to particles with a higher surface charge, like carboxyl-terminated or amine-terminated polystyrene particles [2, 3, 12, 14–17]. In trend, this behavior is reproduced in our simulations. The larger the absolute potential strength U_0, the stronger the hindrance of the diffusion and the stronger the effect of changing the interaction range k, which

can be related to the salt concentration. There is an exception for large particles of diameter $p = 0.9\,b$, where attractive potentials increase the diffusivity in the simulated hydrogel (c.f. section 4.3).

A number of experimental studies have examined the diffusion of 100, 200 and 500 nm sized particles with different kinds of surface chemistry, either mucoinert PEG coating or charged COOH coating, in different kinds of mucus [12, 16, 17, 35, 36]. It was found that the charged COOH coating leads to stronger immobilization of the particle and that in some cases the smallest particles (100 nm) are most efficiently immobilized in mucus, while in other cases it was found that the larger the particle, the stronger is the immobilization. Both situations can be qualitatively reproduced with our model. In fig. 15 we show that particles with a smaller diameter $p = 0.1\,b$ are more efficiently hindered than larger ones with diameter $p = 0.5\,b$. This is because they can get closer to the potential minima in the corners of the simulation box, or, in other words, because larger particles experience a more homogeneous potential than smaller ones. This effect can be observed even better in in fig. 18b, when regarding the data for negative $U_0 = -3,\ -10,\ -20\,k_BT$. Here, one can see that increasing the particle size at a constant interaction range initially leads to an increase in relative diffusivity D/D_0, since the effect of the exponential potential on the diffusing particle decreases. At a certain point the hindrance effect of the steric interactions will become dominant, after which the diffusivity decreases again for increasing particle sizes. At a repulsive interaction potential, i.e. for positive $U_0 = 10,\ 20\,k_BT$ in fig. 18b, the diffusivity decreases for increasing particle size p, due to the effect that both the interaction potential U^{i} and the LJ potential U^{s} are trapping the particle in the center of the simulation box. This situation reproduces the experimentally observed behavior "the bigger the particle, the stronger the immobilization".

To perform a quantitative comparison to the aforementioned experimental results there are some difficulties. The experimental studies do not include any concrete information about the salt concentration inside the mucus which would be needed to compute the interaction range k (c.f. eq. (6)). Furthermore, there are greatly differing suggestions regarding the average mesh size of human mucus ranging from 0.34 µm [13] to 0.8 µm [12]. In fact, it has been reported, that the range of pore openings in human mucus is very broad such that larger particles can travel in regions with larger openings and still be quite mobile inside the mucus, even if they are bigger than the average mesh size [13, 16]. Hence, some assumptions have to be made to be able to draw a closer comparison between simulation and experimental data and we will limit the comparison to two examples.

Example 1 - Larger particles are faster: Lai and coworkers have studied the diffusivity of 100, 200 and 500 nm PEG coated polystyrene particles in undiluted cervicovaginal mucus [12]. To draw a comparison we assume that the interaction range is $k = 0.1\,b$, i.e. small compared to the mesh size, and that the interaction between the hydrogel polymers and the particle is attractive. For attractive interactions ($U_0 < 0$) the dependency of the relative diffusivity D/D_0 in our model is as follows. Smaller particles are strongly hindered due to electrostatic interactions, while larger particles are able to diffuse more freely unless they are of a width comparable to the hydrogel mesh size b, in which case they are immobilized due to steric interaction (c.f. in fig. 18b the data for $U_0 = -10kT$ and $U_0 = -20\,k_BT$). Figure 26a shows how the interaction strengths under study are related to the experimental results by Lai and coworkers. It shows the experimental data and the D/D_0 values for some points along the $U_0 = -10\,k_BT$ and $U_0 = -20\,k_BT$ curves in fig. 18b, which correspond to particles that have a similar size ratio as in the experiment, namely, $p = 0.1, 0.2, 0.5\,b$ and $p = 0.2, 0.4, 0.9\,b$, respectively. The simulation data is in qualitative agreement with the experimental data for the interaction strengths U_0 under study. Hence, according to our simulations, the experimentally observed behavior that small particles are more effectively immobilized could be explained as follows: Regardless of their size, the diffusing particles are immobilized due to attractive electrostatic interactions between particle and mucus fibers. Since experimental data indicates that mucus fibers are rigid [10], small particles might be able to diffuse into regions of stronger electrostatic attraction which larger particles cannot access due to their larger size.

Example 2 - Larger particles are slower: Xu and coworkers have studied the diffusivity of 100, 200, 500, 750 and 1000 nm PEG coated polystyrene particles in fresh bovine vitreus [16]. They report a behavior which is similar to our simulation data for repulsive potentials ($U_0 > 0$). They found that the smaller particles (100 to 500 nm) could equally diffuse relatively freely with relative diffusivities around $D/D_0 = 0.5$. The larger 750 nm and 1000 nm particles were more strongly hindered with $D/D_0 = 0.23$ and 0.014, respectively. Similar behavior is exhibited by our hydrogel model e.g. in fig. 18c which shows the relative diffusivities plotted over the particle diameters p for different U_0 and at an interaction range of $k = 0.2\,b$. The data for attractive potentials $U_0 = 10\,k_BT$ and $U_0 = 20\,k_BT$ shows constant, lightly hindered diffusivity for small particle diameters p and stronger immobilization towards larger particle diameters p. To underline the similarity, in fig. 26b we shows the experimental data by Xu and coworkers in direct comparison to D/D_0 values with similar size ratio ($p = 0.1$, 0.2, 0.5, 0.75 and $1.0\,b$) along the $U_0 = 10\,k_BT$ and $U_0 = 20\,k_BT$ lines in

fig. 18c. This could be interpreted such that all PEGylated nanoparticles experience similar repulsive interaction inside the hydrogel but larger ones with a diameter of more than 500 nm also experience strong steric interactions.

Simulating alternating patches of attractive and repulsive interaction between particle and polymer chain as suggested by Lieleg and coworkers [2, 3] (c.f. section 2.2) leads to results that are qualitatively similar to their experimental findings. Lieleg and coworkers report that the hindrance of positively and negatively charged particles strongly increases for increasing charge, regardless of the sign. In the random charge model (c.f. section 2.2) the diffusivity D/D_0 decreases for increasing absolute interaction strength U_0. This is similar to the experimental findings, since U_0 can be interpreted as the surface charge of the particle diffusing in a heterogeneously charged hydrogel. More concretely, in their 2009 paper, Lieleg and coworkers suggest that selective filtering in the extracellular matrix creates a kind of electrostatic bandpass for particles with small surface charges [3]. They tuned the surface charges of liposomes by varying the mixture of lipids with neutral, positively charged or negatively charged headgroups. The resulting differently charged liposomes were of similar size, between 160 to 170 nm. Lieleg and coworkers found that for increasing negative and positive surface charges, the diffusivities of the liposomes abruptly goes from relatively mobile ($D/D_0 \approx 0.1$) to quasi immobilized ($D/D_0 < 0.0001$). A qualitatively similar immobilization due to strong electrostatic interactions can be found in fig. 23. Here, the random charge hydrogel model is employed so the diffusing particle experiences attraction to some polymer chain patches and repulsion from others, as indicated in fig. 4. As explained in section 2.2, this can be interpreted as a charged particle diffusing inside a heterogeneously charged hydrogel. In such a situation, the particle would experience attraction to some polymer chain patches and repulsion from others, in the case of equal or opposite surface charge sign, respectively. Hence, U_0 can be interpreted as the absolute particle surface charge in the random charge model.

Figure 24 shows that the particle size p dependency for the random charge model is quite similar to the p dependency for attractive potentials, which is presented in fig. 18. Hence, the results by Lai and coworkers [12], who found small particles to be most strongly hindered, can also be compared to the random charge model. In fig. 27 we present a qualitative comparison similar to the example 1 presented above. The experimental data by Lai and coworkers for 100, 200 and 500 nm particles is shown in grey. All simulation data was obtained for an interaction range of $k = 0.1\,b$. As before, the particle diameters were chosen such that they have a similar size ratio as in the experiment, namely, $p = 0.1, 0.2, 0.5\,b$ and $p = 0.2, 0.4, 0.9\,b$ for the $U_0 = 15\,k_BT$

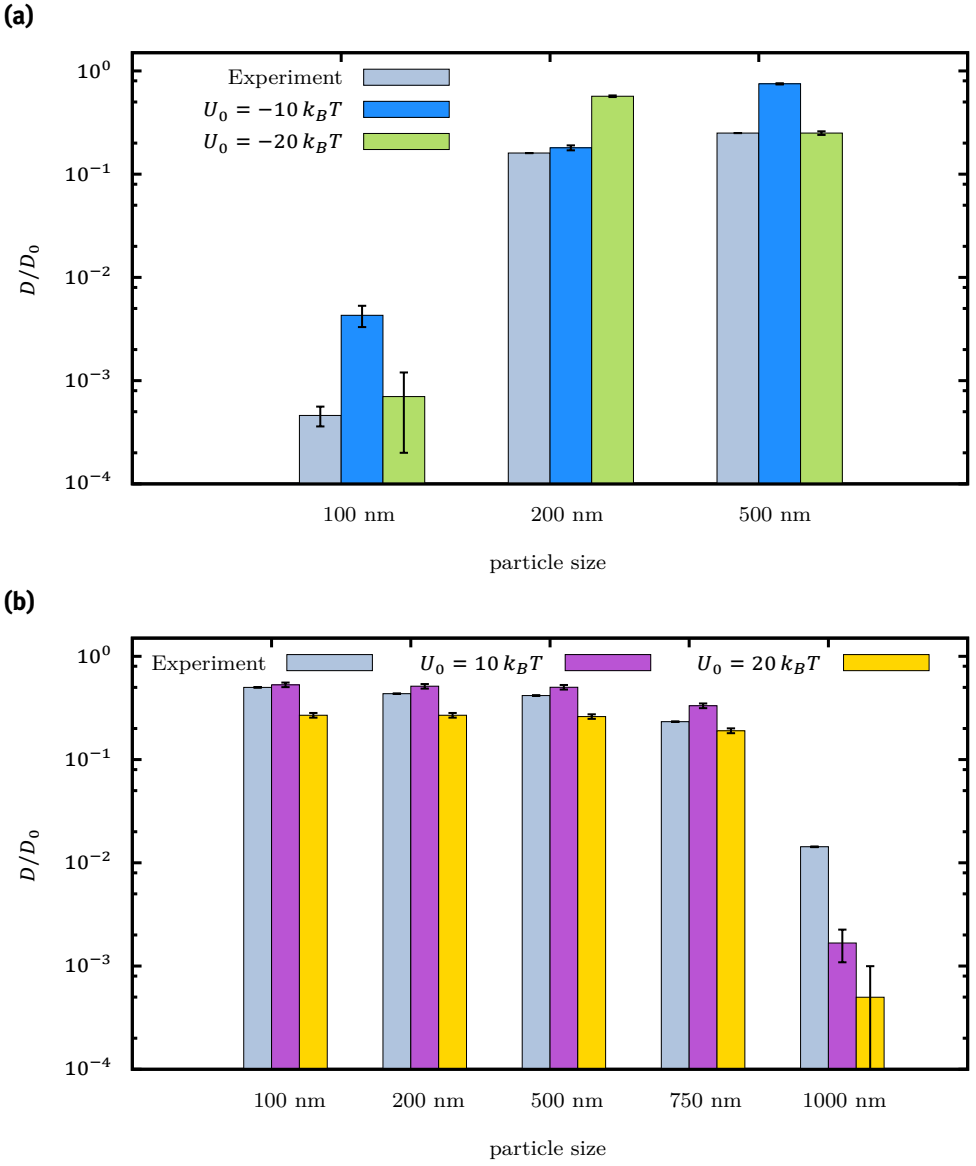

Figure 26. To underline the qualitative similarities between the simulation data and experimental findings the above figures include points from the data published by **(a)** Lai and coworkers [12] and **(b)** Xu and coworkers [16] in grey, and simulation data in color. In **(a)** the simulations data points were obtained at $p = 0.1,\ 0.2,\ 0.5\,b$ and $p = 0.2,\ 0.4,\ 0.9\,b$ for $U_0 = -10\,k_BT$ and $U_0 = -20\,k_BT$, respectively, with the interaction range set to $k = 0.1\,b$. These points can also be found in fig. 18b along the data curves in similar color (i.e. for the same U_0). The particle sizes on the x-axis correspond to the experimental particle sizes. In a similar fashion, in **(b)** the simulation data points were obtained at two different repulsive potentials strengths $U_0 = 10,\ 20\,k_BT$ and $p = 0.1,\ 0.2,\ 0.5,\ 0.75$ and $1.0\,b$ for the 100, 200, 500, 750 and 1000 nm point, respectively. Here, the interaction range was set to $k = 0.2\,b$. The simulation data can be also found in fig. 18c along the curves in similar color (i.e. for the same U_0). Hydrogel model 1 was used for all simulation data shown.

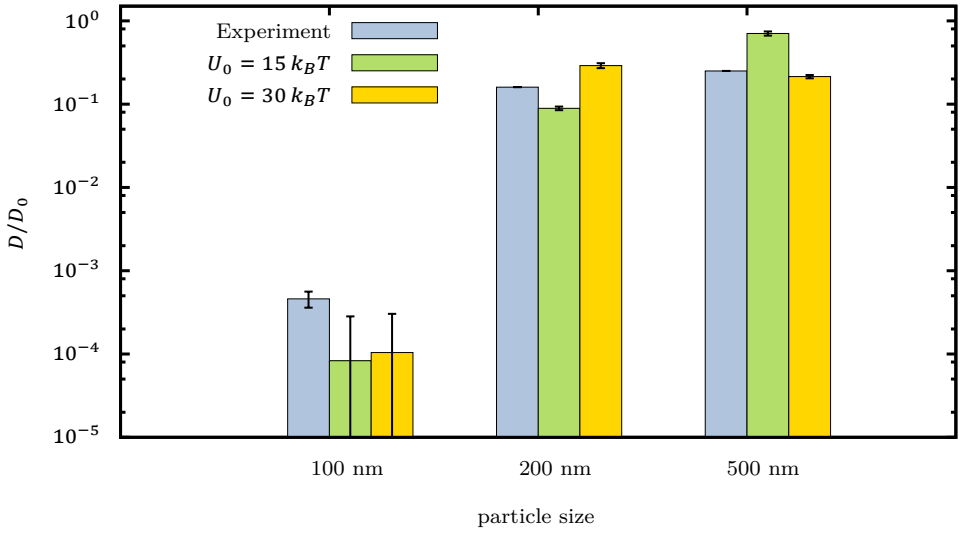

Figure 27. To underline qualitative similarities between the simulation data obtained with the random charge model and experimental findings the above figure includes the data published by Lai and coworkers [12] on the diffusivity of PEG coated polystyrene particles in human mucus in grey and simulation data in color. The simulation data points were obtained for effective particle diameters $p = 0.1,\ 0.2,\ 0.5\,b$ and $p = 0.2,\ 0.4,\ 0.9\,b$ for $U_0 = 15\,k_BT$ and $U_0 = 30\,k_BT$, respectively, with the interaction range set to $k = 0.1\,b$. The simulation data points can also be found in fig. 24 along the curves in similar color (i.e. for the same U_0). The particle sizes on the x-axis correspond to the experimental particle sizes.

data and $U_0 = 30\,k_BT$ data, respectively. There is qualitative agreement between the simulation data and the experiment. Thus, the situation in mucus hydrogels could in fact also be similar to the random charge model, i.e. there could be regions of alternating interaction direction, attractive or repulsive.

Salt Concentration

Making use of eq. (8) the interaction range k can be related to the salt concentration C_{ion}, in that an increase in salt concentration causes a decrease in interaction range k. Lieleg and coworkers found that an increase in salt concentration led to an increase in diffusivity for particles with a charged surface [2]. This increase in diffusivity was not related to a reorganization of the polymer network, but to electrostatic interactions between particle and hydrogel, since neutral particles did not experience such an increase in diffusivity. Such behavior is qualitatively reproduced in our simulations. At stronger potential strengths U_0 particles experience a more drastic increase in relative diffusivity as the interaction range becomes small, i.e. for increasing C_{ion}. To underline this, fig. 28 is presented where the ion concentration dependency of the diffusivity

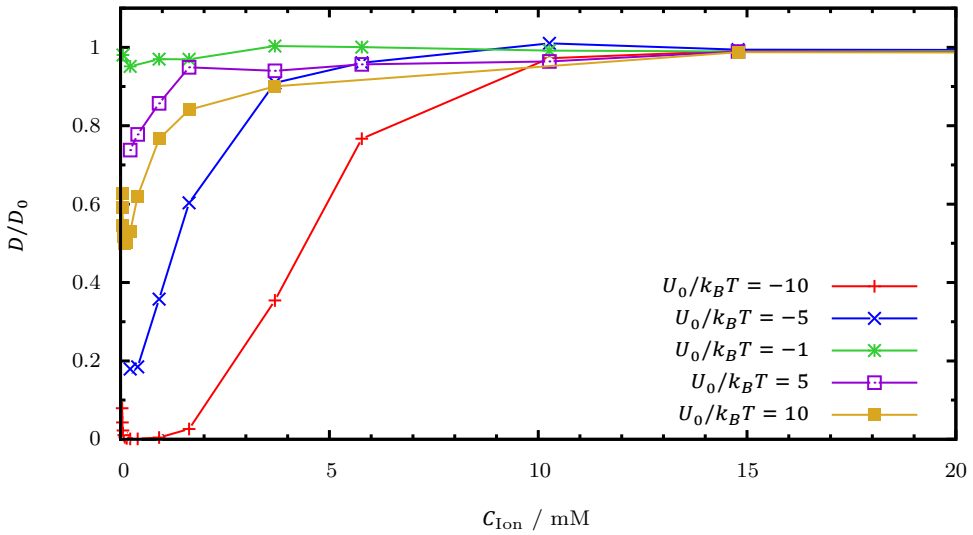

Figure 28. The relative diffusivity D/D_0 in dependence on the ion concentration C_{ion} for different strengths of electrostatic interaction and in a model 1 hydrogel. The scale of the ion concentration corresponds to $p = 10\,\mathrm{nm}$ sized particles diffusing in a hydrogel with a mesh size of $b = 100\,\mathrm{nm}$. The ion concentration is calculated from the interaction range k with eq. (8). The lines are included to guide the eye. D_0 is the free diffusion coefficient.

at different potential strengths is shown for particles of diameter $p = 0.1\,b$. The scale of the ion concentration corresponds to a mesh size of $b = 100\,\mathrm{nm}$. Particles that interact more strongly experience a much stronger increase in diffusivity for increasing salt concentrations, than particles that interact less strongly (e.g. $U_0 = \pm 10\,k_BT$ and $U_0 = \pm 5\,k_BT$, respectively). At increasing ion concentration, the relative diffusivity approaches the value obtained for purely steric hindrance. In the case of attractive electrostatic interactions, i.e. negative U_0, this effect is stronger, since the particles are more effectively immobilized than in the repulsive cases ($U_0 > 0$). For very small ion concentrations there is an increase in diffusivity at $U_0 = -10 k_BT$. This is the same increase in diffusivity that can be seen in the $p = 0.1\,b$ data in fig. 19a for increasing interaction ranges $k \geq 0.2\,b$. One can see in fig. 28, that this increase corresponds to very small salt concentrations $C_{\mathrm{ion}} < 0.5$ mM, which would usually not be present in an experimental situation since biological hydrogels contain ions and experiments with synthetic hydrogels are usually performed in a buffer solution to keep the pH constant.

A quantitative comparison to Jason DeRouchey's experimental data on the salt dependency of Alexa Fluor 488 molecules in dextran hydrogels is described in 5.2.

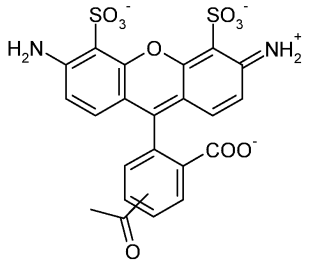

Figure 29. The chemical structure of an Alexa Fluor 488 molecule. The image was taken from `http://patentimages.storage.googleapis.com/WO2010102886A1/imgf000017_0002.png`, accessed March 26, 2014.

5.2 Quantitative Comparison

To determine the correlation length of a dextran hydrogel a simple geometrical assumption was made. It was assumed that the polymer chains form a cubic lattice. This assumption has been deemed reasonable for hydrogels that form tetrafunctional cross-links [8] and it leads to the following equations for determination of the correlation length b, where a is the mean diameter of the dextran monomers, m_a their mass, n_d their number density and N the total number of monomers in volume V:

$$n_d = \frac{N}{V} = \frac{3\, b/a}{b^3} = \frac{3}{ab^2}\,, \tag{24}$$

$$n_d = \frac{(w/v)\%}{100}\frac{1}{m_a}\,, \tag{25}$$

$$\rightarrow\ b = \sqrt{\frac{300\, m_a}{a\,(w/v)\%}}\,. \tag{26}$$

$(w/v)\%$ is the polymer weight per volume percentage with units of grams per milliliters (g/ml) that is used in the unpublished data by Jason DeRouchey, to which we will compare our simulations. The parameters needed for our comparison are $m_a = 162\,\mathrm{Da}$ and $a = 0.39$ nm [26]. At $(w/v)\% = 1$ g/ml the calculated correlation length is $b = 14.4$ nm which is in the same order as determined from experimental data [6,8]. The size of an Alexa 488 particle (c.f. fig. 29) is about 1.5 nm according to Jason DeRouchey [37]. A similar result is obtained, if one adds the bond lengths diagonally along the molecule, 1.2 to 1.5 nm, plus the width of a water molecule, 0.39 nm, to approximately account for hydration. To calculate the salt concentration the formula for the screening length, eq. (6), is used. To compare the experimental and simulation data the radius of the diffusing particle was set to $p = 0.1\, b$ in relative units

which corresponds to $p = 2.2\,\text{nm}$ and a 10 mM offset was added to the calculated ion concentration to include the effect of 10 mM added Tris which was added to the hydrogel solution in the experiment as a buffer. With these parameters the simulation data is in qualitative accordance with the experimental data as shown in fig. 30. The size of the parameter $p = 2.2$ nm can be justified insofar, as it can also be considered as the hydrated particle diameter plus the diameter of the polymer chains, i.e. $(1.5 + 0.4 + 0.4)$ nm $= 2.3$ nm. The calculated correlation length $b = 14.4\,\text{nm}$ and the box size $b = 22\,\text{nm}$, chosen for good agreement between simulation and experiment, are of the same order and thus sufficiently close to each other considering the approximative calculation and the lack of exact experimental data on the dextran correlation length.

Figure 30a shows the comparison between the simulation data and the data by Jason DeRouchey [37] on Alexa 488 diffusion in a dextran hydrogel. The experimental data is indicated by unconnected, filled symbols and the simulation data by connected dots, where the lines are included to guide the eye. The experimental diffusivity is very low for small ion concentrations in the case of a positively charged CM-dextran. Since Alexa 488 has a net negative charge, this data can be compared to the simulation data with $U_0 < 0$, i.e. an attractive interaction potential. One can see, that the simulation data and the experimental data qualitatively agree, although the experimental data approaches a relative diffusivity of $D/D_0 = 0.7$. In the case of a negatively charged and uncharged dextran the diffusivity of similarly charged Alexa 488 remains relatively constant at around $D/D_0 = 0.7$, i.e. the same value which is approached in the case of positively charged dextran. With a repulsive potential of similar strength as in the attractive case, i.e. $U_0 = 7\,k_BT$ the simulation and experimental data agree for large ion concentrations but show different behavior for small ones. Where in the experimental data D/D_0 remains constant towards decreasing C_{Ion}, the simulation data shows a decrease. This effect could just indicate that the interaction strength $U_0 = 7\,k_BT$ was not chosen correctly. The absolute interaction strength in negatively charged CM-dextran could be smaller than the interaction strength in DEAE-dextran which would lead to a flatter simulation data curve. This is indicated in fig. 30a by the data for $U_0 = 1\,k_BT$, for which there is qualitative agreement with the negative CM-dextran as well as uncharged dextran. Hence, our simulation data implies that the reason for the increase in diffusivity of Alexa 488 in positively charged CM-dextran is screening of electrostatic interactions, since that is the underlying effect in the calculation of the interaction range, as explained section 2.4.

Figure 30b shows another comparison between the experiment and the simulation,

but instead of the relative diffusivity D/D_0, the y-axis here corresponds to $D/D_{\text{uncharged}}$, where $D_{\text{uncharged}}$ is the diffusivity of the particle in an uncharged polymer network with purely steric interaction, i.e. at $U_0 = 0$. This way of presenting the data was chosen in order to show how well the shape of the simulation data and experimental curve agree. The differing values for the diffusivity $D_{\text{uncharged}}$ in the experiment and the simulation for increasing ion concentration could be due to further interactions inside the hydrogel, that are not dependent on the ion concentration, like hydrophobic or hydrodynamic interactions. Stylianopoulos and coworkers have found that for a particle that is larger than the fiber diameter, hydrodynamic hindrance can slow the particle more than twofold [27].

Alternatively, it could be due to a systematic underestimation of the steric hindrance effect in our model.

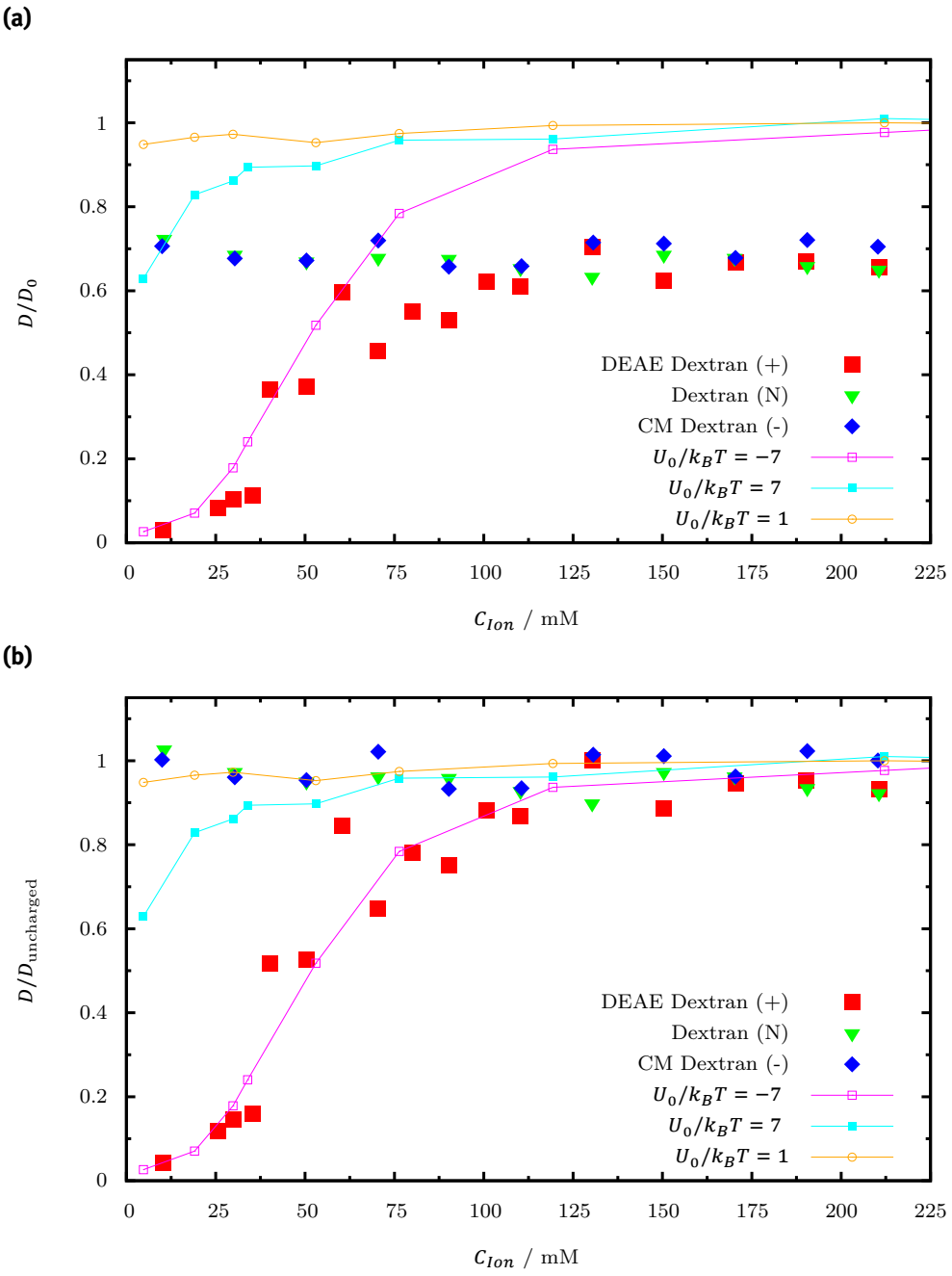

Figure 30. Results on how changing the salt concentration C_{Ion} affects the diffusivity in a particle-hydrogel configuration similar to the experimental setup by Jason DeRouchey [37], with a particle and mesh size of $p = 0.1\,b = 2.2$ nm. The experimental data, indicated by unconnected filled symbols, was supplied by Jason DeRouchey [37] for the diffusion of Alexa Fluor 488 molecules in dextran hydrogels, in 10 mM Tris buffer solution and under varying NaCl concentration. The indicator in brackets indicates the charge of the hydrogel. The lines are included to guide the eye. D_0 is the free diffusion coefficient.

6 Conclusion

The aim of this work was to create a simple model to simulate nanoparticle diffusion in cross-linked hydrogels under consideration of nonsteric interactions between particle and hydrogel. We were able to achieve this by implementing a rigid, cubic periodic lattice to model the hydrogel structure and short-ranged nonsteric interactions via an exponential potential between hydrogel polymer chains and diffusing particle. This sleek model setup enabled the simulations to be computationally inexpensive by focusing on the effect of only a few key parameters like particle size, interaction strength and interaction range. We found that the filtering capability of a hydrogel is strongly influenced by the sign of the interaction potential. There are two underlying processes taking place, which create hindrance due to nonsteric interactions: An attractive interaction potential leads to a *sticking* effect of the particles near the polymer chain intersections at the corners of the simulation box and a repulsive potential leads to a *trapping* effect, where the particle tends to remain in the center of the current simulation box. Both processes hinder the diffusion of particles, but sticking much more than trapping. Thus, if the interaction potential is regarded as electrostatic interaction, we found that the filtering capacity of our simulated hydrogel depends on the sign and strength of the particle charge, in accordance to experimental findings. The random charge model was included to test the effects of an experimentally proposed hydrogel structure with varying patches of different charge. The straight-forward implementation of this model into the existing hydrogel model 1 shows its adaptability. Qualitative agreement between experimental results and our model was found here as well, in that charged particles are strongly immobilized regardless of the sign of their charge, due to a strong sticking effect. Also, the random charge model can be understood as a hydrogel with zero net charge. Thus, the model predicts that even in such a hydrogel immobilization of charged particles may occur.

Combination of steric exclusion and interaction potentials leads to further interesting results. For attractive interaction potentials a maximum in relative diffusivity appears for intermediate particle diameters p. Similar behavior has been observed in some experiments with mucus. Differently sized particles experiencing a repulsive interaction potential exhibit the same diffusivity over a range of different particle sizes. This kind of behavior has also been reported in experimental studies on large nanoparticles in mucus. In the case of purely steric interactions, our model shows a linear dependency on the polymer concentration inside the hydrogel. This is in accordance to some experimental studies, but in other cases a stretched expo-

nential was observed. The variance in the experimental data might arise due to the variable stiffness of different hydrogels. Also, the experimental polymer concentration dependency has, to our knowledge, only been studied for synthetic hydrogels. Michelman-Ribeiro and coworkers state in their 2007 paper that the exponential decrease in nanoparticle diffusivity in gels for increasing polymer concentrations can be attributed to the exponentially increasing bulk viscosity of the gel [32]. Furthermore, Kirch and coworkers [10] have reported that larger particles should be able to locally break up the cross-links between polymer chains in synthetic hydrogels. Since our model hydrogel is immobile and the polymer lattice is stiff, the diffusion of particles larger than b will always be zero. Biopolymer hydrogels, on the other hand, have been reported to form a stiff network. Thus our model might be more applicable here. For future work, it would be interesting to implement a random network with different mesh sizes. This would create a possibility for larger particles to diffuse with nonzero diffusivity and it might lead a different polymer concentration dependency, like the stretched exponential that has been reported in some experimental studies.

As a particularly noteworthy property of our model, we found sticking and trapping to be maximal at intermediate interaction ranges. In the case of electrostatic interactions, the interaction range is related to the salt concentration. We found qualitative agreement between experimental findings and simulation results. Hence, the fact that our model hydrogel has an interaction range dependent filtering sensitivity can be regarded as a prediction which could be investigated in further experimental research.

The fact that our sleek model naturally reproduces experimentally observed behavior is an indicator, that the actual mechanisms governing nanoparticle diffusion in hydrogels can in many cases be boiled down to two essentials: Steric hindrance and electrostatic interaction, where the latter is usually the dominant factor. It would be interesting to test the model with more experimental data like in section 5.2. But at this time we are not aware of any such publications.

To further refine our model, we could include hydrodynamic and hydrophobic interactions. This has been left out so far as to keep the model simple and to avoid overcomplication of the interpretation of the simulation results. Although the results from section 5.2 indicate, that our model might lack such interactions to explain the overestimation of the relative diffusivities at zero interaction potential strength. Another possible refinement of our model could be done for the random charge model. Lieleg and coworkers suggest that the charge distribution along mucin polymer chains might vary for different pH-values [2]. At neutral pH, there are varying patches of

weak positive, weak negative and neutral charge. At high pH, the charge patches along the polymer chain become predominantly negatively charged or neutral. Our random charge model could be adjusted to simulate such a situation, but more detailed experimental data would be needed for a comparison.

For the research on nanoparticle diffusion in biopolymer hydrogels for medical applications our research provides interesting insights. Our model predicts that the mobility of nanoparticles is strongly dependent on electrostatic interactions. Thus, by increasing the salt concentration or the pH it should be possible to release, for example, drugs from a hydrogel carrier.

References

[1] O. Lieleg and K. Ribbeck, "Biological hydrogels as selective diffusion barriers.," *Trends in cell biology*, vol. 21, pp. 543–51, Sept. 2011.

[2] O. Lieleg, I. Vladescu, and K. Ribbeck, "Characterization of particle translocation through mucin hydrogels," *Biophysical journal*, vol. 98, pp. 1782–9, May 2010.

[3] O. Lieleg, R. Baumgärtel, and A. Bausch, "Selective filtering of particles by the extracellular matrix: an electrostatic bandpass," *Biophysical journal*, vol. 97, pp. 1569–77, Sept. 2009.

[4] S. Lai, Y. Wang, D. Wirtz, and J. Hanes, "Micro-and macrorheology of mucus," *Advanced drug delivery reviews*, vol. 61, no. 2, pp. 86–100, 2009.

[5] A. Vashist, A. Vashist, Y. K. Gupta, and S. Ahmad, "Recent advances in hydrogel based drug delivery systems for the human body," *Journal of Materials Chemistry B*, vol. 2, p. 147, Dec. 2014.

[6] W. Hennink, H. Talsma, J. Borchert, S. De Smedt, and J. Demeester, "Controlled release of proteins from dextran hydrogels," *Journal of Controlled Release*, vol. 39, no. 1, pp. 47–55, 1996.

[7] W. M. Saltzman, M. L. Radomsky, K. J. Whaley, and R. A. Cone, "Antibody diffusion in human cervical mucus.," *Biophysical journal*, vol. 66, pp. 508–15, Feb. 1994.

[8] B. Amsden, "An Obstruction-Scaling Model for Diffusion in Homogeneous Hydrogels," *Macromolecules*, vol. 32, pp. 874–879, Feb. 1999.

[9] S. P. Zustiak, H. Boukari, and J. B. Leach, "Solute diffusion and interactions in cross-linked poly(ethylene glycol) hydrogels studied by Fluorescence Correlation Spectroscopy.," *Soft matter*, vol. 6, pp. 3609–3618, Aug. 2010.

[10] J. Kirch, A. Schneider, B. Abou, A. Hopf, U. F. Schaefer, M. Schneider, C. Schall, C. Wagner, and C.-M. Lehr, "Optical tweezers reveal relationship between microstructure and nanoparticle penetration of pulmonary mucus.," *Proceedings of the National Academy of Sciences of the United States of America*, vol. 109, pp. 18355–60, Nov. 2012.

[11] T. Canal and N. A. Peppas, "Correlation between mesh size and equilibrium degree of swelling of polymeric networks.," *Journal of biomedical materials research*, vol. 23, pp. 1183–93, Oct. 1989.

[12] S. K. Lai, D. E. O'Hanlon, S. Harrold, S. T. Man, Y.-Y. Wang, R. Cone, and J. Hanes, "Rapid transport of large polymeric nanoparticles in fresh undiluted human mucus," *Proceedings of the National Academy of Sciences of the United States of America*, vol. 104, no. 5, pp. 1482–1487, 2007.

[13] S. K. Lai, Y.-Y. Wang, K. Hida, R. Cone, and J. Hanes, "Nanoparticles reveal that human cervicovaginal mucus is riddled with pores larger than viruses.," *Proceedings of the National Academy of Sciences of the United States of America*, vol. 107, pp. 598–603, Jan. 2010.

[14] Y. Cu and W. M. Saltzman, "Mathematical modeling of molecular diffusion through mucus," *Advanced Drug Delivery Reviews*, vol. 61, no. 2, pp. 101–114, 2009.

[15] X. Yang, K. Forier, L. Steukers, S. Van Vlierberghe, P. Dubruel, K. Braeckmans, S. Glorieux, and H. J. Nauwynck, "Immobilization of pseudorabies virus in porcine tracheal respiratory mucus revealed by single particle tracking.," *PloS one*, vol. 7, p. e51054, Jan. 2012.

[16] Q. Xu, N. J. Boylan, J. S. Suk, Y.-Y. Wang, E. A. Nance, J.-C. Yang, P. J. McDonnell, R. A. Cone, E. J. Duh, and J. Hanes, "Nanoparticle diffusion in, and microrheology of, the bovine vitreous ex vivo," *Journal of Controlled Release*, vol. 167, no. 1, pp. 76–84, 2013.

[17] B. S. Schuster, J. S. Suk, G. F. Woodworth, and J. Hanes, "Nanoparticle diffusion in respiratory mucus from humans without lung disease," *Biomaterials*, vol. 34, no. 13, pp. 3439–3446, 2013.

[18] M. Allen and D. Tildesley, *Computer simulation of liquids*. Oxford, UK: Clarendon Press, 1987.

[19] Y. Wu, S. Joseph, and N. R. Aluru, "Effect of cross-linking on the diffusion of water, ions, and small molecules in hydrogels.," *The journal of physical chemistry. B*, vol. 113, pp. 3512–20, Mar. 2009.

[20] S. S. Jang, W. A. Goddard, and M. Y. S. Kalani, "Mechanical and transport properties of the poly(ethylene oxide)-poly(acrylic acid) double network hydrogel from molecular dynamic simulations.," *The journal of physical chemistry. B*, vol. 111, pp. 1729–37, Feb. 2007.

[21] S. Edgecombe, S. Schneider, and P. Linse, "Monte Carlo Simulations of Defect-Free Cross-Linked Gels in the Presence of Salt," *Macromolecules*, vol. 37, pp. 10089–10100, Dec. 2004.

[22] P. A. Netz and T. Dorfmüller, "Computer simulation studies of diffusion in gels: Model structures," *The Journal of Chemical Physics*, vol. 107, p. 9221, Dec. 1997.

[23] P. Licinio and A. Teixeira, "Anomalous diffusion of ideal polymer networks," *Physical Review E*, vol. 56, pp. 631–634, July 1997.

[24] T. Miyata, A. Endo, and T. Ohmori, "Brownian dynamics simulation study of self-diffusion of a charged particle in swollen counter-charged hydrogel modeled as cubic lattice," *Journal of Chemical Engineering of Japan*, vol. 35, no. 7, pp. 640–648, 2002.

[25] H. Zhou and S. Chen, "Brownian dynamics simulation of tracer diffusion in a cross-linked network," *Physical Review E*, vol. 79, p. 021801, Feb. 2009.

[26] L. Johansson, C. Elvingson, and J. E. Loefroth, "Diffusion and interaction in gels and solutions. 3. Theoretical results on the obstruction effect," *Macromolecules*, vol. 24, pp. 6024–6029, Oct. 1991.

[27] T. Stylianopoulos, M.-Z. Poh, N. Insin, M. G. Bawendi, D. Fukumura, L. L. Munn, and R. K. Jain, "Diffusion of particles in the extracellular matrix: the effect of repulsive electrostatic interactions.," *Biophysical journal*, vol. 99, pp. 1342–9, Sept. 2010.

[28] M. Jardat, B. Hribar-Lee, and V. Vlachy, "Self-diffusion of ions in charged nanoporous media," *Soft Matter*, vol. 8, no. 4, p. 954, 2012.

[29] J. Israelachvili, *Intermolecular and Surface Forces*. Intermolecular and Surface Forces, Elsevier Science, 2010.

[30] M. Matsumoto and T. Nishimura, "Mersenne twister: a 623-dimensionally equidistributed uniform pseudo-random number generator," *ACM Transactions on Modeling and Computer Simulation*, vol. 8, pp. 3–30, Jan. 1998.

[31] T. Williams, C. Kelley, and many others, "Gnuplot 4.4: an interactive plotting program." `http://gnuplot.sourceforge.net/`, March 2010.

[32] A. Michelman-Ribeiro, F. Horkay, R. Nossal, and H. Boukari, "Probe diffusion in aqueous poly(vinyl alcohol) solutions studied by fluorescence correlation spectroscopy.," *Biomacromolecules*, vol. 8, pp. 1595–600, May 2007.

[33] G. Modesti, B. Zimmermann, M. Börsch, A. Herrmann, and K. Saalwächter, "Diffusion in Model Networks as Studied by NMR and Fluorescence Correlation Spectroscopy.," *Macromolecules*, vol. 42, pp. 4681–4689, July 2009.

[34] Y. Wang, S. Lai, and J. Suk, "Addressing the PEG mucoadhesivity paradox to engineer nanoparticles that "slip" through the human mucus barrier," *Angewandte Chemie International Edition*, pp. 9726–9729, 2008.

[35] J. S. Suk, S. K. Lai, Y.-Y. Wang, L. M. Ensign, P. L. Zeitlin, M. P. Boyle, and J. Hanes, "The penetration of fresh undiluted sputum expectorated by cystic fibrosis patients by non-adhesive polymer nanoparticles.," *Biomaterials*, vol. 30, pp. 2591–7, May 2009.

[36] S. K. Lai, J. S. Suk, A. Pace, Y.-Y. Wang, M. Yang, O. Mert, J. Chen, J. Kim, and J. Hanes, "Drug carrier nanoparticles that penetrate human chronic rhinosinusitis mucus.," *Biomaterials*, vol. 32, pp. 6285–90, Sept. 2011.

[37] J. DeRouchey, "Probe and PAMAM diffusion in neutral polymer gels,"

STATUTORY DECLARATION

I declare that I have authored this thesis personally and independently, that I have not used any aids other than the declared sources / resources, and that I have explicitly marked all material which has been quoted either literally or by content from the used sources.

date: .....

signature: .....

EIDESSTATTLICHE ERKLÄRUNG

Ich erkläre an Eides statt, dass ich die vorliegende Arbeit selbstständig verfasst, andere als die angegebenen Quellen/Hilfsmittel nicht benutzt, und die den benutzten Quellen wörtlich und inhaltlich entnommenen Stellen als solche kenntlich gemacht habe.

Ort, Datum: .....

Unterschrift: .....